# A THEORETICAL AND EXPERIMENTAL INVESTIGATION OF THE ANNULAR JET GROUND EFFECT MACHINE

by

William Alexander Graham, Jr.

First Lieutenant, U. S. Army

Thesis submitted to the Graduate Faculty of the

Virginia Polytechnic Institute

in candidacy for the degree of

MASTER OF SCIENCE

in

Aeronautical Engineering

December 1960

Blacksburg, Virginia

TABLE OF CONTENTS

# LIST OF TABLES AND FIGURES

## TABLES



## FIGURES

## NOMENCLATURE

| | |
|---|---|
| $A$ | Lift augmentation ratio due to ground effect |
| $A_B$ | Area of ground effect machine base ($= \pi \frac{D_i^2}{4}$) |
| $A_j$ | Area of annular nozzle |
| $b$ | Length of two-dimensional ground effect machine base |
| $C$ | Absolute velocity of annular jet |
| $C_A$ | Velocity at any point along "wall A" (see Figure 4b) |
| $(C_P)_{avg}$ | Average value of pressure coefficient across jet at nozzle (see page 28) |
| $(C_{P_A})_{avg}$ | Average value of pressure coefficient on "wall A" (see Figure 4b and page 28) |
| $D$ | Diameter of the annular jet |
| $D_i$ | Inside diameter of the annular nozzle |
| $D_O$ | Outside diameter of the annular nozzle |
| $F_j$ | Jet thrust from the annular nozzle |
| $h$ | Height of the ground effect machine base above the ground |
| $p$ | Static pressure |
| $P$ | Total pressure |
| $P_B$ | Total pressure on the base of the ground effect machine |
| $P_O$ | Ambient pressure |
| $q$ | Dynamic pressure ($= \rho \frac{C^2}{2}$) |
| $r$ | Radius of the annular jet at any point across the jet thickness |
| $R$ | Radius of curvature of the annular jet in a meridian plane |

| | |
|---|---|
| $R_a$ | Value of the radius of curvature (R) at the outside streamline of the annular jet |
| $R_B$ | Value of R at the inside streamline of the annular jet |
| $R_i$ | Inside radius of the annular nozzle (value of r at $D_i$) |
| $R_o$ | Outside radius of the annular nozzle (value of r at $D_o$) |
| $R^*$ | Value of r at a point where the jet static pressure reaches the ambient value |
| t | Thickness of the annular jet at the nozzle |
| $U_o$ | Velocity of the jet at a point where the static pressure reaches the ambient value (at R*)(see Figure 4) |
| V | Theoretical velocity of the jet in the ground effect machine upstream (at "infinity") from the nozzle exit (see Figure 4b) |
| $\theta_o$ | Angle between the direction of the annular jet and the vertical in a meridian plane (see Figure 1a) |
| $\rho$ | Density of the air |

## SUBSCRIPTS

| | |
|---|---|
| a | Refers to the streamline adjoining ambient air |
| A | Refers to the inner streamline of the Schwarz-Christoffel diagram |
| avg | Refers to average values |
| B | Refers to the base of the ground effect machine |
| 0 | Refers to ambient |
| des | Refers to design value(s) (out of "ground effect") |
| gro | Refers to value(s) in "ground effect" |
| Z | Refers to values in the physical (Z) plane |
| $\zeta$ | Refers to values in the transform ($\zeta$) plane |

# I. INTRODUCTION

"Ground effect" is not a new expression. The term defines the cushioning effect of the ground on a lifting surface such as a wing or helicopter rotor, and has been known and utilized (on occasion) for some fifty years. Only very recently, however, has the aviation industry become actively interested and engaged in designing and building vehicles which actually utilize the ground effect principle as their principle means of sustaining flight.

The almost universally used parameter in evaluating the performance of any ground effect machine has been the "augmentation factor", i.e., the ratio of the actual lifting capacity of the jet nozzle close to the ground to a given reference lifting capacity. This ratio has been defined in many ways, usually in terms of an infinitely "thin" jet of air from the annular nozzle; i.e., it is assumed that the velocity and pressure do not vary across the jet and that $D_i \approx D_o$ (see Figure 1). This assumption was made for simplification; however, it is not an accurate physical description.

Recently Pinnes (reference 6) has developed a more realistic "thick jet" analysis for the augmentation ratio in which he assumes flow variations across the jet. His theory, however, is only valid down to a height (h) above the ground equal to the jet thickness (t). Many ground effect machines will probably operate primarily in this height range of $h \leq t$ and indeed, will not be able to "fly" much higher (reference 5). In this thesis, a two-dimensional theory

is developed using the Schwarz-Christoffel conformal transformation. This theory is applicable in the region where $h \leq t$ as well as for $h > t$. The theory is an exact potential flow analysis of the flow in a "levapad" type of vehicle (see Figures 2 and 4a) which has been modified to approximate the annular jet (Figure 4b). In addition to the theoretical study, experimental augmentation ratios are developed for an axi-symmetric annular jet and for a two-dimensional "levapad." Experimental plots of augmentation factor versus $\frac{h}{D_j}$ (or $\frac{h}{b}$) are compared for various types of model configurations, and are compared with the theoretical curves obtained in this thesis and those in reference 6. Studies carried out to ascertain the effect of varying the center body geometry show that proper internal design will make a significant difference in the augmentation ratio obtained.

Flow visualization studies are made for the models tested using nylon tufts (see Section XI). In general the flow patterns are found to bear out the predictions made in references 2 and 6; and, a discrepancy in the assumption of "ideal jet flow" in reference 2, which is noted from these studies is discussed in the flow visualization section.

## II. REVIEW OF LITERATURE

Perhaps a clear cut definition of a ground effect machine is in order before proceeding further. Boehler (reference 1), in 1958, defined this as; "A device which, at least in one phase of its operation, derives a substantial portion of its support from a cushion of high-pressure air sealed between the base of the machine and the ground. This seal can be realized practically by means of a peripheral high speed jet (annular jet) or by means of a labyrinth." This definition however, did not include the air bearing type of machine such as the plenum chamber or the "levapad" currently under development by Ford Motor Company. In addition it did not reflect upon today's requirements for high forward speed, but only emphasized the hovering characteristics of such machines. As a result of this, Boehler has recently revised his definition to read: "A ground effect machine is a surface vehicle operating in close proximity to the earth's surface (over land or water), however never touching it, except at rest, being separated from it by a cushion or film of air, however thin. Ground friction being considerably reduced as compared to a conventional surface vehicle, it depends entirely upon aerodynamic forces for propulsion and for control. Maximum forward speed is therefore not limited any more by ground friction or water wave resistance; but as for an aircraft, by air drag." Since there are no wheels, tracks, screws, or rudders, the ground effect machine is primarily a problem for the aerodynamicist rather than the automotive or marine engineer.

Both the military services and civilian industry have recently become quite interested in the development of these vehicles. One of their more obvious advantages is their ability to do the work of a truck, a ship, and an airplane. The ground cushion phenomena today is feasible and may be applied practically as an effective rough terrain vehicle. Special emphasis is being placed on Ground Effects Take Off and Landing (GETOL) by both the Navy and Army. Military interest in ground effect vehicles has so far been primarily restricted to the peripheral jet type of machine (see Figure 2). This vehicle operates on the principle that in proximity to the ground, a pressure bubble (or air cushion) is developed in the cavity bounded by a jet sheet, the base of the machine, and the ground. This air cushion gives support to the machine.

The Ford Motor Company is interested in another type of ground effect machine referred to as the "levapad." In the simple "levapad" high pressure air is injected centrally between a smooth pad (or base) and the ground (which must also be reasonably smooth), this film of air acting like a lubricant. At present the "levapad" is contemplated only for use with rail systems (reference 1). Other concepts for ground effect machines include: the ram wing (the operation of a wing in very close proximity to the ground); the plenum chamber (which may resemble an inverted bathtub), currently under study by Bell Aircraft Company; the labyrinth seal, which is a viscous-flow recirculating system; and the diffuser, another recirculating system under

study by Hiller Aircraft. Several of these vehicle types are illustrated in Figure 2. Only the "levapad" and peripheral jet will be discussed in this thesis, with attention directed chiefly to the latter. It is believed that the peripheral jet type of ground effect machine offers the best compromise between versatility, simplicity, and performance.

Until recently the generally accepted three-dimensional expression for an augmentation factor was that developed by Chaplin (reference 2), in which he assumed an ideal jet flow (a thin, non-mixing jet). For this type of flow it is assumed that $\frac{R_o}{R_i} \approx 1$ (see Figure 1), that there is no variation of flow properties across the jet, and that the jet does not entrain any of the surrounding air. That is, the "ideal" jet becomes tangent to the ground without having a stagnation point; whereas a stagnation point would result if some of the air were fed back into the cavity to replace any air entrained in the "real" jet (see Figure 3). Using a simple momentum analysis Chaplin derived the following expression for augmentation ratio,

$$A = \cos \theta_o + \frac{1 - \sin \theta_o}{\frac{2h}{R_o}} \tag{1}$$

or specialized for a vertical jet $(\theta_o = 0^\circ)$,

$$A = 1 + \frac{1}{\frac{2h}{R_o}} = 1 + \frac{1}{\frac{4h}{D_o}} \tag{2}$$

Recently Pinnes (reference 6) has developed a new expression

for the augmentation ratio, again assuming an ideal, inviscid fluid with no mixing, but assuming a free vortex flow and variations of pressure and velocity across the jet proper. This is now known as a "thick jet" analysis because of the variation of flow properties across the jet. Pinnes' definition of augmentation ratio is (see Figure 1 for nomenclature);

$$A = \frac{1}{2}\left[1 - \left(\frac{R_a}{R_B}\right)^2\right]\frac{A_B}{A_j} + \frac{\cos\theta_o}{2}\left(\frac{R_a}{A_B} + 1\right) \qquad (3)$$

This "thick jet" expression can be related to the "thin jet" analysis as follows:

Noting that $$A_B = \frac{\pi}{4} D_i^2 \qquad (4)$$

and $$A_j = \frac{\pi}{2}(D_o + D_i)\, t \qquad (5)$$

and letting $$\theta_o = 0 \text{ or } \cos\theta_o = 1$$

so that $$(R_B)_{\theta_o = 0} = h \qquad (6)$$

and $$(R_a)_{\theta_o = 0} = h - t \ , \qquad (7)$$

then, combining equations (4), (5), (6) and (7) with (3) one obtains,

$$A_{\theta_o = 0} = \frac{1}{2}\left[1 - \frac{(h-t)^2}{h^2}\right]\frac{\frac{\pi}{4} D_i^2}{\frac{\pi}{2}(D_o + D_i)\, t} + \frac{1}{2}\left(\frac{h-t}{h} + 1\right)$$

$$= \frac{1}{4h}\left(2 - \frac{t}{h}\right)\frac{D_i^2}{(D_o + D_i)} + \frac{2h - t}{2h} \ . \qquad (8)$$

Now making Chaplins' "thin jet" assumptions,

namely, $$t \approx 0 \qquad (9)$$

and $$D \approx D_o \approx D_i \approx \frac{1}{2}(D_o + D_i) \tag{10}$$

then $$A_{\theta_o = 0} = \frac{1}{2h} \frac{\frac{1}{4}(D_o + D_i)^2}{D_o + D_i} + 1$$

$$= 1 + \frac{1}{4 \frac{h}{D_o}} \tag{11}$$

which is identical with equation (2).

It should be noted that Pinnes' "thick jet" analysis is only valid down to an operating height of $h = t$. At this point, according to the assumption that $C = C_a \frac{R_a}{R}$, $R_a$ would become zero and the velocity can not be defined at $h \leq t$; thus the theory is not valid in this region.

An attempt is made in this thesis to develop a "thick jet" analysis that does not lose its validity in the above-mentioned region.

## III. A NEW THEORETICAL EXPRESSION FOR LIFT AUGMENTATION RATIO FOR THE TWO DIMENSIONAL GROUND EFFECT MACHINE

The existing theories for augmentation ratio and their shortcomings have been briefly discussed in Section II. A need exists for a two-dimensional theory based on a realistic "thick jet" analysis that is valid throughout the entire range of operating heights. This will entail using an approach different from that of Pinnes for analyzing the variation of velocity and pressure across the jet.

A new "thick jet" analysis for the lift augmentation ratio will be developed, using an approach which is different from those of references 2 and 6. In this analysis it is assumed that the two dimensional annular jet can be simulated by taking one half of a "levapad" (see Figure 4a), the flow of which is divided symmetrically by a vertical streamline. This is in contrast to the previously used assumption of 'no stagnation point on the ground.' The dividing streamline can be regarded as a bounding wall since no flow can cross it. The resulting fluid motion is believed to be a good approximation to a two-dimensional annular jet.

The Schwarz-Christoffel Transform, a conformal transformation, is well suited to this type of analysis and is utilized here to study the flow field. It allows one to transform the bounding walls of the modified "levapad" (diagram) into the "real" axis of the complex "$\zeta$" plane and the internal flow into

the upper half of the $\zeta$ plane. Using principles of hydrodynamics and complex variables the flow is then analyzed in this plane. The pressure and velocity at a given point can be determined for the flow in the $\zeta$ plane and then transferred back to the original "Z" plane. In the analysis the flow is necessarily assumed to be non-viscous, incompressible, and non-mixing (i.e., an ideal fluid flow).

A "levapad" diagram has been modified (Figures 4, 4a and 4b) to approximate a cross-section (in two dimensions) of an annular jet. The centerline or dividing streamline BC of the "levapad" is coincident with the "inner" streamline (the streamline next to the base cavity) of the simulated annular jet. If the fluid flow around the "corner" resulting from this modification can be analyzed using potential flow theory, it is believed that the resulting solution will be a good approximation to the flow of an annular jet in "ground effect."

We will denote a vertical velocity ( at "infinity") by V, and a horizontal velocity (at "infinity") by $U_o$ . Ultimately we hope to obtain an expression from which the local velocity at any point can be evaluated, in the flow field, in terms of the important ratio of height of base to jet thickness $(\frac{h}{t})$. For reasons to become apparent later we will define that portion of the "inner" streamline, BC, extending from zero height (ground plane) to height = h, as "wall A." The figure is seen to be a simple polygon with vertices (A,F) and (C,D) at infinity (see Figure 4b).

The interior angles at points B and E will be denoted as $\beta$ and $\gamma$, respectively.

In the hope that the problem will be easier to solve in a half plane we now proceed to set up the Schwarz-Christoffel transformation which maps the polygonal boundary described above, in the "Z" plane, into the real axis of the "$\zeta$" plane. With the aid of this transformation the pressure distribution will be obtained, and from this the velocity distribution for the flow field.

The points A and F (which are coincident at "infinity") will be mapped into the origin of the $\zeta$ plane. The fluid flow is assumed to be uniform at this point in the physical (Z) plane. The point B is chosen to map into the point (-1,0) in the $\zeta$ plane. Point E is mapped into the point $(a,0)$ in the $\zeta$ plane; where $a$ is a quantity to be determined later. The infinity points C and D will map into negative and positive infinity, respectively, in the $\zeta$ plane. It is known that the angle $\alpha$, at $(A,F)_{Z_\infty}$, is equal to zero. The interior angles $\beta$ and $\gamma$ are seen to be $\frac{\pi}{2}$ and $\frac{3\pi}{2}$, respectively.

Now the Schwarz-Christoffel transformation for this configuration is defined as (see reference 4);

$$\frac{dZ}{d\zeta} = K\,(\zeta - E)^{\frac{\gamma}{\pi} - 1}\,(\zeta - B)^{\frac{\beta}{\pi} - 1}\,(\zeta - A)^{\frac{\alpha}{\pi} - 1} \qquad (12)$$

where K is a complex constant to be determined. Since $a$, -1, and 0 are the values of $\zeta$ corresponding to vertices E, B, and A of the polygon in the Z plane, equation (12) can be written as,

$$\frac{dZ}{d\zeta} = K(\zeta - a)^{\frac{1}{2}}(\zeta + 1)^{-\frac{1}{2}}(\zeta)^{-1} = \frac{K}{\zeta}\left(\frac{\zeta - a}{\zeta + 1}\right)^{\frac{1}{2}} \qquad (13)$$

Assuming a uniform flow at C,D in the physical (Z) plane as emanating from a source at infinity of output Vt, then, the uniform flow at A,F is due to a sink of equal strength (at infinity). Under a conformal transformation a source or sink at a given point corresponds to an equal source or sink at the image of that point. Thus, there must be a sink in the $\zeta$ plane at the origin which takes in a volume "Vt", per unit time, over an angle of $\pi$. The quantity $\frac{Vt}{\pi}$ is known as the "sink strength." Note that the source at $Z_{C,D}$ must transform into a source at infinity in the $\zeta$ plane.

In order to simplify the determination of the quantities K and $a$ we shall proceed at once to the use of the complex potential function (w) for the flow. As is well known, for a sink at the origin in the $\zeta$ plane,

$$w = (\text{sink strength})(\ln \zeta) = \frac{Vt}{\pi} \ln \zeta \qquad (14)$$

Now it follows that in the $\zeta$ plane the complex conjugate velocity

$$\frac{dw}{d\zeta} = \frac{Vt}{\pi\zeta} = (u - iv)_\zeta \qquad (15)$$

where u and v are the horizontal and vertical components of the resultant velocity, respectively, in that plane. Since the complex conjugate velocity in the Z plane is obtained from

$$\frac{dw}{dZ} = \frac{dw}{d\zeta}\,\frac{d\zeta}{dZ} \tag{16}$$

then (13) and (15) can be combined to give

$$\frac{dw}{dZ} = \frac{Vt}{\pi\zeta}\,\frac{\zeta}{K}\left(\frac{\zeta+1}{\zeta-a}\right)^{\frac{1}{2}} = \frac{Vt}{\pi K}\left(\frac{\zeta+1}{\zeta-a}\right)^{\frac{1}{2}} = (u - iv)_{Z} \tag{17}$$

In order to evaluate $K$, note that:

$$\text{At vertex C, } (u - iv)_{Z_C} = iV, \text{ where } u = 0,\ v = -V; \tag{18}$$

but $\zeta_C = -\infty$,

so at $Z = Z_C$ and $\zeta = \zeta_C$, combining (17) and (18) yields,

$$\left(\frac{dw}{dZ}\right)_{Z_C} = (u - iv)_{Z_C} = iV = \frac{Vt}{\pi K}\left[\frac{1+\frac{1}{\zeta}}{1-\frac{a}{\zeta}}\right]_{\zeta=-\infty} = \frac{Vt}{\pi K}$$

or $$K = -\frac{it}{\pi} \tag{19}$$

Now, to further simplify the determination of $a$, introduce (from continuity considerations) the relation,

$$Vt = U_o h, \text{ or } U_o = \frac{Vt}{h} \tag{20}$$

where necessarily it is assumed that the density remains constant.

Note that at vertex A, $(u - iv)_{Z_A} = U$, where $u = U,\ v = 0$; (21)

but $$\zeta_A = 0,$$

so on combining (17) and (20), obtain,

$$\left(\frac{dw}{dZ}\right)_{Z_A} = (u - iv)_{Z_A} = \frac{Vt}{h} = \frac{Vt}{\pi K}\left(\frac{\zeta + 1}{\zeta - a}\right)^{\frac{1}{2}}_{\zeta_A = 0} \quad . \tag{22}$$

thus, $$\frac{Vt}{h} = \frac{Vt}{\pi}\ \frac{i\pi}{t}\left(\frac{1}{-a}\right)^{\frac{1}{2}}$$

which reduces to,

$$a = \left(\frac{h}{t}\right)^2 \quad , \tag{23}$$

Now, combining (13) and (19) we can define the Schwarz-Christoffel transform as;

$$\frac{dZ}{d\zeta} = \frac{-it}{\pi}\left(\frac{\zeta - a}{\zeta + 1}\right)^{\frac{1}{2}} \quad . \tag{24}$$

To obtain an explicit relationship between $Z$ and $\zeta$ one must integrate equation (24), an expression which is rather cumbersome to handle in its present form. To facilitate the integration of $\frac{dZ}{d\zeta}$ we will introduce the following coordinate transformation;

$$\zeta = \frac{1 + b^2\tau^2}{\tau^2 - 1} \quad \text{or} \quad \tau^2 = \frac{1 + \zeta}{\zeta - b^2} \tag{25}$$

where

$$b^2 = a = \left(\frac{h}{t}\right)^2 \tag{26}$$

and hence,

$$\frac{d\zeta}{d\tau} = \frac{-2\tau(b^2 + 1)}{(\tau^2 - 1)^2} \quad .$$

now, $$\frac{dw}{d\tau} = \frac{dw}{d\zeta}\frac{d\zeta}{d\tau} = \frac{2ik(b^2+1)}{\pi(1+b^2\tau^2)(\tau^2-1)}$$

or $dw = \frac{2ik}{\pi}\frac{b^2+1}{(b^2\tau^2+1)(\tau^2-1)}d\tau$ which may be

written as, $$dw = \frac{2ik}{\pi b^2}\frac{b^2+1}{(\tau^2+\frac{1}{b^2})(\tau^2-1)}d\tau \quad . \qquad (29)$$

The above expression may be simplified further by the use of partial fractions to give

$$dw = \frac{2ik}{\pi b^2}\left[\frac{-b^2}{\tau^2+\frac{1}{b^2}} + \frac{b^2}{2}\frac{1}{\tau-1} - \frac{b^2}{2}\frac{1}{\tau+1}\right]d\tau \quad . \qquad (30)$$

Equation (30) can be readily integrated to yield,

$$w = \frac{-2ik}{\pi}b\tan^{-1}b\tau + \frac{ik}{\pi}\ln\left(\frac{\tau-1}{\tau+1}\right) + I \qquad (31)$$

where I is a constant of integration to be determined.

Equations (29) and (30) will now combine to yield,

$$w = \frac{-2ik}{\pi}\tan^{-1}\frac{b}{1}\tau + \frac{ik}{\pi}\ln\left(\frac{\tau-1}{\tau+1}\right) + I \quad . \qquad (32)$$

In order to evaluate I note that at vertex B,

$$w_B = 0 \text{ and } \zeta_B = -1 \qquad (33)$$

Hence, $\tau^2 = 0$, so that from equation (30),

$$z = 0 = \frac{-2ih}{\pi} \tan^{-1}(0) + \frac{it}{\pi} \ln(-1) - \frac{it}{\pi} \ln(1) + L$$

$$= \frac{it}{\pi}(i\pi) + L = -t + L$$

or $L = t$ .

Hence, equation (30) is now written as,

$$z = \frac{-2ih}{\pi} \tan^{-1} \frac{h}{t}\tau + \frac{it}{\pi} \ln\left(\frac{\tau - 1}{\tau + 1}\right) + t$$

or

$$z = \frac{h}{\pi} \ln\left(\frac{1 - i\frac{h}{t}\tau}{1 + i\frac{h}{t}\tau}\right) + \frac{it}{\pi} \ln\left(\frac{\tau - 1}{\tau + 1}\right) + t \quad , \qquad (32)$$

which is the Schwarz-Christoffel transformation for the problem considered here. We are now able to map any point on the $\zeta$ plane into the $z$ plane, using the coordinate transformation in equation (29).

Next we will determine the speed at points in the flow field. In terms of the complex potential $w$ the speed $q_z$ is defined as;

$$q_z = \left|\frac{dw}{dz}\right| \qquad (33)$$

Combining equations (17), (19), and (33) yields

$$q_z = V\left|\frac{\zeta + 1}{\zeta - a}\right|^{\frac{1}{2}} \qquad (34)$$

We are now able to introduce the coefficient of pressure $(C_p)$

which can be defined in terms of $q_z$ and $U_o$. Employing the incompressible Bernoulli equation and the definition of pressure coefficient, it can be shown that

$$C_P = 1 - \left(\frac{q_z}{U_o}\right)^2 \tag{35}$$

Combining equations (20), (34), and (35) yields,

$$C_P = 1 - \left(\frac{h}{t}\right)^2 \left|\frac{\zeta + 1}{\zeta - a}\right| \text{ or, } C_P = 1 - \left(\frac{h}{t}\right)^2 \left|\tau^2\right| \tag{36}$$

The pressure distribution can now be determined for any part of the flow field for any desired $\frac{h}{t}$ ratio. Now calling $q_z = C$ (to be consistent with notation used elsewhere in this thesis), then, from (35),

$$C_P = 1 - \frac{C^2}{U_o^2} \text{ or } C^2 = (1 - C_p)\, U_o^2 , \tag{37}$$

Thus the velocity at any point on the modified "levapad" flow diagram can be determined in terms of the pressure coefficient, which in turn can be defined in terms of the $\frac{h}{t}$ ratio, as seen in equation (36).

For the "two-dimensional" ground effect machine, the lift augmentation ratio is defined as,

$$A = \frac{(F_j)_{gro} + b\,(P_B - P_0)}{(F_j)_{des}} \tag{38}$$

where the jet thrust from a vertical two-dimensional annular nozzle

(see Figure 4) operating out of ground effect can be expressed as,

$$(F_j)_{des} = 2\rho V^2 \int_0^t dt = 2\rho V^2 t \ . \tag{39}$$

Here $V$ represents the constant velocity at the nozzle exit, and the "2" has been employed to account for both jets. The jet thrust from the nozzle in ground effect is defined as,

$$(F_j)_{gro} = 2\rho \int_0^t c^2 \, dt + 2 \int_0^t (p - p_0) \, dt \ . \tag{40}$$

But, from the incompressible Bernoulli equation,

$$p - p_0 = \frac{1}{2}\rho (U_0^2 - c^2) \tag{41}$$

where $U_0$ is the horizontal velocity at "infinity" (see Figure 4), so that

$$2 \int_0^t (p - p_0) \, dt = 2 \left(\frac{1}{2}\rho U_0^2 t - \frac{1}{2}\rho \int_0^t c^2 \, dt\right)$$

and thus

$$(F_j)_{gro} = 2\rho \int_0^t c^2 \, dt + \rho U_0^2 t - \rho \int_0^t c^2 \, dt$$

$$= \rho \int_0^t c^2 \, dt + \rho U_0^2 t \ . \tag{42}$$

Now let $p_A$ denote the static pressure at any point along wall A

(Figure 4b), and let $C_A$ denote the corresponding local velocity. Again employing the Bernoulli equation, one finds that

$$p_A = p_0 + \frac{1}{2}\rho (U_0^2 - C_A^2) \quad . \tag{43}$$

Now assume $p_B$ is constant and equals $(p_A)_{avg}$, where $(p_A)_{avg}$ is taken to be

$$(p_A)_{avg} = \frac{\int_0^h p_A \, dh}{h} = p_B$$

then

$$p_B = \frac{1}{h}\left\{\int_0^h \left(p_0 + \frac{1}{2}\rho \left[U_0^2 - C_A^2\right]\right) dh\right\}$$

$$= p_0 + \frac{1}{2}\rho U_0^2 - \frac{\rho}{2h}\int_0^h C_A^2 \, dh$$

or

$$p_B - p_0 = \frac{1}{2}\rho U_0^2 - \frac{\rho}{2h}\int_0^h C_A^2 \, dh \quad . \tag{44}$$

We can now write equation (38) as,

$$A = \frac{\rho\int_0^t C^2 \, dt + \rho U_0^2 t + b\left(\frac{1}{2}\rho U_0^2 - \frac{\rho}{2h}\int_0^h C_A^2 \, dh\right)}{2\rho V^2 t}$$

$$= \frac{\int_0^t C^2 \, dt}{2V^2 t} + \frac{U_0^2}{2V^2} + \frac{b}{4}\frac{U_0^2}{V^2 t} - \frac{b\int_0^h C_A^2 \, dh}{4h V^2 t} \quad . \tag{45}$$

but from (20) $U_0^2 = V^2 \left(\frac{t}{h}\right)^2$ , then

$$A = \frac{1}{2V^2}\left(\frac{\int_0^t C^2\,dt}{t} - \frac{b\int_0^h C_A^{\,2}\,dh}{2ht}\right) + \frac{1}{2}\left[\left(\frac{t}{h}\right)^2 + \frac{b}{2t}\left(\frac{t}{h}\right)^2\right]$$

or

$$A = \frac{1}{2}\frac{t^2}{h^2 U_0^2}\left(\frac{\int_0^t C^2\,dt}{t} - \frac{b\int_0^h C_A^{\,2}\,dh}{2ht}\right) + \frac{1}{2}\left(\frac{t}{h}\right)^2\left(1 + \frac{b}{2t}\right) \qquad (46)$$

From (37) it is noted that $C^2 = (1 - C_P)\,U_0^2$ .

Hence,

$$\int_0^t C^2\,dt = \int_0^t (1 - C_P)\,U_0^2\,dt = U_0^2\left(t - \int_0^t C_P\,dt\right) \qquad (47)$$

and similarly

$$\int_0^h C_A^{\,2}\,dh = U_0^2\left(h - \int_0^h C_{P_A}\,dh\right) \qquad (48)$$

where $C_{P_A}$ is the pressure coefficient at any point on wall A.

Equations (47) and (48) can be readily evaluated for any $\frac{h}{t}$ ratio by graphically integrating the pressure distribution curves obtained from the Schwarz-Christoffel transform. Now, combining (46), (47), and (48) it follows that

$$A = \frac{1}{2U_0^2}\left(\frac{t}{h}\right)^2 \left[\frac{U_0^2\left(t - \int_0^t C_P\, dt\right)}{t} - \frac{b\, U_0^2\left(h - \int_0^h C_{P_A}\, dh\right)}{2ht}\right]$$

$$+ \frac{1}{2}\left(\frac{t}{h}\right)^2 \left[1+\left(\frac{b}{2t}\right)\right]. \qquad (49)$$

Finally, defining

$$(C_P)_{avg} = \frac{\int_0^t C_P\, dt}{t} \quad \text{and} \quad (C_{P_A})_{avg} = \frac{\int_0^h C_{P_A}\, dh}{h}$$

the expression for augmentation ratio becomes;

$$A = \frac{1}{2}\left(\frac{t}{h}\right)^2 \left[2 - (C_P)_{avg} + \frac{b}{2t}(C_{P_A})_{avg}\right] \qquad (50)$$

Equation (50) is a new approximation for the augmentation ratio of a "two-dimensional" annular jet ground effect machine. It is based on an inviscid "thick jet" analysis, and is valid in the height range of $h \leq t$, as well as $h > t$. As previously mentioned, the thick jet theory developed in reference 6 is not valid in the region below $h = t$.

## IV. A NEW THREE DIMENSIONAL THEORY FOR LIFT AUGMENTATION RATIO OF THE ANNULAR JET

Having obtained a theoretical expression for lift augmentation ratio in two dimensions, using a "thick jet" analysis, the expression will now be extended for an approximation to the three-dimensional or axi-symmetric case.

Defining the augmentation ratio, in general, as

$$A = \frac{(F_j)_{gro} + A_B (P_B - P_0)}{(F_j)_{des}} \quad . \tag{51}$$

Where the thrust from a vertical annular nozzle out of ground effect will be defined as

$$(F_j)_{des} = \rho V^2 \int_{R_i}^{R_0} \int_0^{2\pi} r dr d\theta = \pi \rho V^2 (R_0^2 - R_i^2) \; . \tag{52}$$

The thrust for a nozzle in ground effect can be defined as,

$$(F_j)_{gro} = \rho \int_{R_i}^{R_0} \int_0^{2\pi} C^2 \, r dr d\theta + \int_{R_i}^{R_0} \int_0^{2\pi} (p - p_0) \, r dr d\theta$$

$$= 2\pi\rho \int_{R_i}^{R_0} C^2 \, r dr + 2\pi \int_{R_i}^{R_0} (p - p_0) \, r dr$$

But, following (41), $(p - p_0) = \frac{1}{2} \rho (U_0^2 - C^2)$ (assuming $U_0 > 0$), then

$$2\pi \int_{R_i}^{R_0} (P - P_0)\, rdr = 2\pi \int_{R_i}^{R_0} \left[\frac{1}{2} \rho (U_0^2 - C^2)\right] rdr$$

$$= \pi \rho U_0^2 \frac{(R_0^2 - R_i^2)}{2} -$$

$$- \pi \rho \int_{R_i}^{R_0} C^2\, rdr \quad .$$

Finally, it is observed that

$$(F_j)_{gro} = \pi \rho \int_{R_i}^{R_0} C^2 rdr + \frac{\pi \rho U_0^2 (R_0^2 - R_i^2)}{2} \qquad (53)$$

Now, from equation (44),

$$P_B - P_0 = \frac{1}{2} \rho U_0^2 - \frac{\rho}{2h} \int_0^h C_A^2\, dh$$

Noting that, $$A_B = \frac{\pi D_i^2}{4}$$

the augmentation ratio can be written as,

$$A = \frac{\pi\rho \int_{R_i}^{R_o} C^2 r dr + \frac{\pi\rho U_o^2 (R_o^2 - R_i^2)}{2}}{\pi\rho V^2 (R_o^2 - R_i^2)}$$

$$+ \frac{\frac{\pi D_i^2}{4} (\frac{1}{2}\rho U_o^2 - \frac{\rho}{2h} \int_0^h C_A^2 dh)}{\pi\rho V^2 (R_o^2 - R_i^2)}$$

$$= \frac{\int_{R_i}^{R_o} C^2 r dr}{V^2 (R_o^2 - R_i^2)} + \frac{U_o^2}{2V^2} + \frac{D_i^2}{8} \frac{U_o^2}{V^2 (R_o^2 - R_i^2)}$$

$$- \frac{D_i^2 \int_0^h C_A^2 dh}{8h V^2 (R_o^2 - R_i^2)} \quad . \tag{54}$$

Now, the continuity equation can be written as (see Figure 4),

$$2\pi\rho \int_{R_i}^{R_o} C r dr = 2\pi\rho V \int_{R_i}^{R_o} r dr = 2\pi\rho R^* U_o h$$

or,

$$\int_{R_i}^{R_o} C r dr = \frac{V (R_o^2 - R_i^2)}{2} = R^* U_o h \quad . \tag{55}$$

Combining (54) and (55) yields,

$$A = \frac{\int_{R_i}^{R_0} C^2 \, r dr}{V^2 (R_0^2 - R_i^2)} + \frac{(R_0^2 - R_i^2)^2}{8 (R^* h)^2}$$

$$+ \frac{D_i^2}{32} \frac{R_0^2 - R_i^2}{(R^* h)^2} - \frac{D_i^2 \int_0^h C_A^2 \, dh}{8h V^2 (R_0^2 - R_i^2)} \qquad (56)$$

Now, referring to equations (37) and (55), one can define,

$$\frac{\int_0^h C_A^2 \, dh}{h} = (C_A^2)_{avg} = \left[1 - (C_{P_A})_{avg}\right] U_0^2$$

$$= \left[1 - (C_{P_A})_{avg}\right] \frac{V^2 (R_0^2 - R_i^2)^2}{4 (R^* h)^2} \; . \qquad (57)$$

Combining (54) and (57) yields

$$A = \frac{R_0^2 - R_i^2}{8 (R^* h)^2} \left[R_0^2 - R_i^2 + \frac{(D_i)^2}{4} (C_{P_A})_{avg}\right]$$

$$+ \frac{\int_{R_i}^{R_0} C^2 \, r dr}{V^2 (R_0^2 - R_i^2)} \qquad (58)$$

but, from (37),

$$C^2 = (1 - C_p)\, U_0^2$$

so

$$\int_{R_i}^{R_0} C^2\, r dr = U_0^2 \left[ \int_{R_i}^{R_0} r dr - \int_{R_i}^{R_0} C_p\, r dr \right]$$

$$= U_0^2 \left[ \frac{R_0^2 - R_i^2}{2} - \int_{R_i}^{R_0} C_p r dr \right], \tag{59}$$

Combining (58) and (59) yields,

$$A = \frac{R_0^2 - R_i^2}{8\,(R^* h)^2} \left[ 2\,(R_0^2 - R_i^2) + \frac{D_i^2}{4} (C_{P_A})_{avg} \right.$$

$$\left. - 2 \int_{R_i}^{R_0} C_p\, r dr \right] \tag{60}$$

We now define,

$$\frac{\int_{R_i}^{R_0} C_p\, r dr}{t} = (C_p r)_{avg}$$

Hence, (60) reduces to,

$$A = \frac{(R_0^2 - R_i^2)}{8\,(R^* h)^2}\left[2\,(R_0^2 - R_i^2) + \frac{D_i^2}{4}\,(C_{P_A})_{avg} - 2t\,(C_P\, r)_{avg}\right] \tag{61}$$

But

$$R_0^2 - R_i^2 = (R_0 - R_i)\,(R_0 + R_i) = t\,(R_0 + R_i)$$

So (61) can be written as,

$$A = \frac{1}{8}\,\frac{t}{h}\,\frac{R_0 + R_i}{R^*}\left[2\,t\,\frac{R_0 + R_i}{R^* h} + \frac{D_i}{4R^*}\,\frac{D_i}{h}\,(C_{P_A})_{avg} - \frac{2\,t\,D_i}{R^* h}\,\frac{(C_P r)_{avg}}{D_i}\right] \tag{62}$$

On the basis of an order of magnitude analysis we will now assume,

$$R_0 = 0\,[R_i] \quad \text{or} \quad R_0 + R_i \approx 2\,R_i \quad . \tag{63}$$

While this appears to be identical with the "thin jet" assumption of equation (10), it is important to note that the assumption in (63) will have negligible effect upon the magnitude of equation (62), and that (62) is based upon results of the "thick jet" analysis of the last section. Combining (62) and (63) yields,

$$A = \frac{1}{4}\left[4\left(\frac{t}{h}\right)^2\left(\frac{R_i}{R^*}\right)^2 + \frac{1}{4}\left(\frac{D_i}{h}\right)^2 \frac{t}{R^*}\,\frac{R_i}{R^*}\,(C_{P_A})_{avg} - 2\left(\frac{t}{h}\right)^2 \frac{R_i\, D_i}{(R^*)^2}\,\frac{(C_P r)_{avg}}{D_i}\right]$$

Or, since $D_i = 2 R_i$

Then,

$$A = \frac{1}{4}\left[\left(\frac{t}{h}\right)^2 \left(\frac{D_i}{R^*}\right)^2 + \frac{1}{8}\left(\frac{D_i}{h}\right)^2 \frac{t}{R^*}\frac{D_i}{R^*}\left(C_{P_A}\right)_{avg} - \left(\frac{t}{h}\right)^2 \left(\frac{D_i}{R^*}\right)^2 \frac{(C_{P^r})_{avg}}{D_i}\right] \tag{64}$$

We will now make the further assumption that,

$$\frac{D_i}{R^*} \approx n \frac{h}{t} \tag{65}$$

since we know that physically, $R^*$ varies inversely with the $\frac{h}{t}$ ratio. The factor $n$ is a variable that will be determined from an examination of the experimental data. Now, combining (64) and (65) yields,

$$A = \frac{1}{4} n^2 \left[1 + \left(\frac{1}{8}\right)\left(\frac{D_i}{t}\right)\left(C_{P_A}\right)_{avg} - \frac{(C_{P^r})_{avg}}{D_i}\right]. \tag{66}$$

In order that equation (66) correspond as closely as possible with the plots of the experimental data, we will define,

$$n^2 = \exp\left(3.35 - 23.2 \frac{t}{D_i}\right) .$$

The above relation was determined by plotting a "desired" $n^2$ (different for each $\frac{t}{D_i}$) versus all $\frac{t}{D_i}$ ratios tested. The resulting plot was seen to approximate a logarithmic curve, and the above

empirical equation for $n^2$ was obtained through "curve fitting" methods. Thus, equation (66) becomes,

$$A = \frac{1}{4}\left[\exp\left(3.35 - 23.2\,\frac{t}{D_i}\right)\right]\left[1 + \frac{1}{8}\,\frac{D_i}{t}\,(C_{P_A})_{avg} - \left(\frac{C_{Pr}}{D_i}\right)_{avg}\right] \tag{67}$$

Equation (67) is a semi-empirical approximation for the augmentation ratio of an axi-symmetric ground effect machine. It was adapted from the two-dimensional theory derived in the previous section. Necessarily this expression is useful only when $R_0 - R_i$ is small and the jet is located at a large distance from the center of the machine, i.e., $(R_0 - R_i) \ll D_i$ .

## V. DESCRIPTION OF TEST APPARATUS

The three-dimensional and two-dimensional experiments were conducted using the static test stands shown in Figures 5 and 6, respectively. The three-dimensional body shell was constructed of molded fiberglass, and is 12.75 inches in diameter at the open end. The intake nozzle was fashioned from oak and bonded to the fiberglass shell. A cast iron $1\frac{1}{4}$ inch pipe fitting was bonded to the intake end of the nozzle, to insure that there would be no air leakage upstream from the nozzle exit. Air, under pressure, entered through a $1\frac{1}{4}$ inch line connected to a shop supply rated at 100 PSIG. In the inlet a full length X-shaped vane was installed to keep the flow uniform and to reduce turbulence. Two centerbodies, fashioned from pine, were used interchangeably (see Figures 7 and 8). One centerbody was hemispherically shaped, to maintain a constant one inch spacing between the centerbody and the shell; the other was of an arbitrary design thereby allowing an investigation for two types of internal flow geometry to be carried out. Balsa vanes were attached to both centerbodies (see Figure 7), again to reduce turbulence and to insure a uniform distribution of flow about the exit periphery. The annular nozzle thickness was varied by using three interchangeable skirt rings, fashioned from pine, having inside diameters of 11.98 inch, 12.28 inch, and 12.53 inch respectively (see Figures 9 and 10). The two thickest rings (used to obtain the thinnest nozzles openings) were slightly curved on the inside face and making a 30 degree angle with the

vertical at the exit. In all, with the two centerbodies and three nozzle rings, plus a "no centerbody" configuration, seven different variations in model geometry were used for comparative purposes. The annular nozzle thicknesses available were: 0.625 inches ($\frac{t}{D_i} = 0.053$), 0.375 inches ($\frac{t}{D_i} = 0.032$), and 0.075 inches ($\frac{t}{D_i} = 0.006$). Eight machine screws $1\frac{1}{4}$ inches by $\frac{1}{8}$ inch were equally spaced around the periphery of the shell to hold the nozzle rings in place and to hold the base plate in position. These also allowed fine adjustments to be made so that the slot width around the machine was held constant. The ground plane was simulated by a circular shaped piece of plate glass 29 inches in diameter, backed by a piece of $\frac{1}{2}$ inch plywood of the same diameter, and mounted on a metal shaft which was free to slide in a metal tube fixed to the table. The height of the ground plane could be adjusted (to any desired position) by sliding this mount up and down in the tube. The shaft was positioned by means of a hydraulic jack.

The two-dimensional "levapad" model (see Figure 6) was constructed from fir material and mounted on a seven by four foot piece of plywood. The "slot" thickness was 1.7 inches without spacers. When wooden spacers were inserted, the slot thickness was reduced to 0.625 inches. The ground plane was simulated by a 42 inch by 2 inch block which could be adjusted to any "height" below the base. The entire apparatus was covered with a sheet

of $\frac{1}{4}$ inch plexiglass for visualization purposes. The plexiglass and ground plane were held at their desired position by means of clamps. It was also found necessary to attach the plexiglass to the model itself in order to insure no leakage of air. In this respect plexiglass was found to be superior to plate glass and, indeed, allowed for excellent visual and photographic observation. Modeling clay was used to seal any exposed cracks between surfaces on both the two-dimensional and three-dimensional models. Air was supplied to the "levapad" model from the same 100 PSIG supply mentioned before, but through a standard $\frac{1}{2}$ inch air line.

## VI. INSTRUMENTATION OF TEST APPARATUS

The three-dimensional model was equipped with a total pressure probe and a static pressure tap located in the air line just above the inlet nozzle (see Figure 11). A pressure survey was made across the inlet with the single total pressure probe at various arbitrary air flow settings. The resulting curves were graphically integrated, and in all cases the integrated average total pressure was found to agree with the actual pressure measured at approximately a constant position in the inlet. The total pressure probe was then permanently affixed at the position where average pressures were apparent, to be used in measuring the total intake nozzle pressure. The dynamic pressure at the annular nozzle outlet was measured, at various stations across and around the nozzle exit, by a pitot-static tube (see Figure 12). The base plate, made from $\frac{1}{8}$ inch brass plate was instrumented with 89 flush-mounted pressure taps and leads (see Figure 13). The taps were arranged in five concentric circles of different radii, and one tap was located at the center of the base plate. The leads extended through hollow wooden channels upward through the shell, and were connected to a manometer board for pressure measurement readings. The base plate pressures obtained could then be integrated to determine the "lifting force" on the vehicle in ground effect.

The two-dimensional model was equipped with a total pressure probe and a static pressure tap in the inlet nozzle (see Figure

14). Dynamic pressures at the exit nozzle were obtained with a total pressure probe and a static pressure tap, both fitted into the nozzle close to the exit proper. One of the two base plates was instrumented with 31 flush mounted pressure taps and leads. The pressure leads extended through slots cut in the plywood baseboard, and were connected to a manometer board for pressure measurements. Since the model was symmetric, it was not necessary to instrument both base plate surfaces.

## VII. PROCEDURE

Seven separate model configurations were used in the three-dimensional model tests. Tests were conducted for the range $0.011 \leq \frac{h}{D_i} \leq 0.126$ for each configuration. The ratio of total inlet nozzle pressure to atmospheric pressure was kept at a constant value of 1.02, for all $\frac{h}{D_i}$, and for all test runs, to approximate the performance of a fan being used rather than a shop air supply (see DISCUSSION Section). During each test run the 89 pressure readings (measured on the manometer boards) were recorded. The average dynamic pressures at the annular nozzle exit were determined by making pressure surveys across the jet for each test run (i.e., for each $\frac{h}{D_i}$ tested) and at several peripheral stations.

The two-dimensional "levapad" model employed two different configurations; the 1.7 inch exit nozzle ($\frac{t}{b} = 0.067$) and the 0.625 inch exit nozzle ($\frac{t}{b} = 0.025$), (see Figure 4a for notation). The total inlet nozzle pressure was again held at a constant ratio with respect to local atmospheric pressure for each set of test "runs." A pressure ratio of 1.005 was employed with the 1.7 inch nozzle configuration, while the 0.625 inch nozzle allowed a pressure ratio of 1.02 to be maintained. Dynamic pressures at the exit nozzle were measured for all $\frac{h}{b}$ values tested.

## VIII. AN EXPERIMENTAL AUGMENTATION RATIO FOR THE AXI-SYMMETRIC GROUND EFFECT MACHINE

Having obtained theoretical augmentation ratio expressions for the simulated two-dimensional and the three-dimensional annular jet machines, an expression for the ratio of the three-dimensional annular jet will now be obtained, to be used in evaluating experimental data. Empirical curves will be plotted, to be compared with the theoretical expressions previously discussed.

Defining the augmentation ratio as:

$$A = \frac{(F_j)_{gro} + A_B \int_0^{R_i} \int_0^{2\pi} (P_B - P_0)\, r dr d\theta}{(F_j)_{des}} \tag{68}$$

then out of ground effect, for any fixed value of $\theta_0$ (see Figure 1a for definition of $\theta_0$)

$$(F_j)_{des} = \left[ \rho (C^2)_{des} \int_{R_i}^{R_0} \int_0^{2\pi} r dr d\theta \right] \cos \theta_0$$

where $(C^2)_{des}$ can be considered constant, and $r$ is a radial position in the annular jet. Hence,

$$(F_j)_{des} = \left[ \pi \rho (C^2)_{des} (R_0^2 - R_i^2) \right] \cos \theta_0 \tag{69}$$

In ground effect, for any fixed $\theta_0$ ,

$$(F_j)_{gro} = \left[\rho\int_{R_i}^{R_0}\int_0^{2\pi}(c^2)_{gro}\, r\,dr\,d\theta + \int_{R_i}^{R_0}\int_0^{2\pi}(p - p_0)\, r\,dr\,d\theta\right]\cos\theta_0$$

$$= \left[2\pi\rho\int_{R_i}^{R_0}(c^2)_{gro}\, r\,dr + 2\pi\int_{R_i}^{R_0}(p - p_0)\, r\,dr\right]\cos\theta_0 \qquad (70)$$

where $(c^2)_{gro}$ is the square of the jet velocity for the machine operating in ground effect.

Hence,

$$\frac{(F_j)_{gro}}{(F_j)_{des}} = \frac{2\rho\int_{R_i}^{R_0}(c^2)_{gro}\, r\,dr + 2\int_{R_i}^{R_0}(p - p_0)\, r\,dr}{\rho(c^2)_{des}(R_0^2 - R_i^2)}$$

Now, define

$$(c^2)_{avg} = \frac{2\int_{R_i}^{R_0}(c)^2\, r\,dr}{R_0^2 - R_i^2} \quad \text{and}$$

$$q = \frac{1}{2}\rho(c^2)_{avg} = \frac{2\int_{R_i}^{R_0}\frac{\rho c^2}{2}\, r\,dr}{R_0^2 - R_i^2}$$

then,

$$\frac{(F_j)_{gro}}{(F_j)_{des}} = \frac{(q)_{gro}}{(q)_{des}} + \frac{\int_{R_i}^{R_o} (p - p_o)\, rdr}{(q)_{des}\,(R_o^2 - R_i^2)} \tag{71}$$

where $(q)_{gro}$ is the dynamic pressure of the jet for the machine operating in ground effect.

Now the quantity

$$\frac{A_B \int_0^{R_i} \int_0^{2\pi} (P_B - P_o)\, rdrd\theta}{(F_j)_{des}}$$

$$= \frac{\frac{\pi}{4} D_i^2 \int_0^{R_i} \int_0^{2\pi} (P_B - P_o)\, rdrd\theta}{\pi\rho (c^2)_{des}\,(R_o^2 - R_i^2)\cos\theta_o}$$

$$= \frac{D_i^2 \int_0^{R_i} \int_0^{2\pi} (P_B - P_o)\, rdrd\theta}{8\,(q)_{des}\,(R_o^2 - R_i^2)\cos\theta_o}$$

and the augmentation ratio can be written as

$$A = \left[ \frac{(q)_{gro}}{(q)_{des}} + \frac{\int_{R_i}^{R_o} (p - p_o)\, rdr}{(q)_{des}\,(R_o^2 - R_i^2)} \right]$$

$$+ \frac{D_i^2}{8\,(q)_{des}} \frac{\int_0^{R_i} \int_0^{2\pi} (P_B - P_o)\, rdrd\theta}{(R_o^2 - R_i^2)\cos\theta_o} \qquad (72)$$

The first and second terms of equation (72) can be determined by graphical integration of the pressures measured across the jet proper. The last term of the equation will be determined by graphically integrating the pressures obtained from the 89 stations in the centerbody base plate.

The results obtained from the collection of experimental data can be seen in Tables I and II; and, the augmentation ratio curves are plotted in Figures 21 through 29, for the various configurations tested.

## IX. AN EXPERIMENTAL EXPRESSION FOR LIFT AUGMENTATION RATIO, AS APPLIED TO THE "LEVAPAD"

The analysis in Section III (equation (50)) gave an approximation for the two-dimensional annular jet. However, since the analysis was actually made using half of a "levapad" (diagram), it was felt that an interesting comparison might be made by actually determining the augmentation ratio for a two-dimensional "levapad." In order to make such a comparison the augmentation ratio will now be developed for this configuration model.

Defining the augmentation ratio as

$$A = \frac{(F_j)_{gro} + 2\,b \int_0^1 (P_B - P_0)\, d\,\frac{x}{b}}{(F_j)_{des}} \tag{73}$$

where $b$ is the "base" dimension.

Note: The unit width base has an area of $2\,b$ due to symmetry (see Figure 4a). Also, the nozzle thickness will be denoted as $2\,t$ to be consistent with previous notation.

The jet thrust out of ground effect can be defined as

$$(F_j)_{des} = \rho\,(C^2)_{des} \int_{-t}^{t} dt = 2\rho(C^2)_{des}\, t\ . \tag{74}$$

The thrust in ground effect can be expressed as

$$(F_j)_{gro} = \rho \int_{-t}^{t} (C^2)_{gro}\, dt + \int_{-t}^{t} (P - P_0)\, dt$$

$$= 2\rho \left[ (c^2)_{gro} \right]_{avg} t + \int_{-t}^{t} (p - p_0)\, dt \qquad (75)$$

where

$$\left[ (c^2)_{gro} \right]_{avg} = \frac{\int_{-t}^{t} c^2\, dt}{2t}$$

Now the ratio

$$\frac{(F_j)_{gro}}{(F_j)_{des}} = \frac{2\rho \left[ (c^2)_{gro} \right]_{avg} t + \int_{-t}^{t} (p - p_0)\, dt}{2\rho (c^2)_{des}\, t}$$

$$= \frac{(q)_{gro}}{(q)_{des}} + \frac{\int_{-t}^{t} (p - p_0)\, dt}{4 (q)_{des}\, t} \qquad (76)$$

where $(q)_{gro}$ is the dynamic pressure of the jet operating in ground effect and $(q)_{des}$ is the dynamic pressure of the jet operating out of ground effect.

The term,

$$\frac{2\,b\int_0^1 (P_B - P_0)\,d\frac{x}{b}}{(F_J)_{des}} = \frac{2\,b\int_0^1 (P_B - P_0)\,d\frac{x}{b}}{2\rho(c^2)_{des}\,t}$$

$$= \frac{b\int_0^1 (P_B - P_0)\,d\frac{x}{b}}{2\,(q)_{des}\,t} \qquad (77)$$

so that finally

$$A = \frac{(q)_{gro}}{(q)_{des}} + \frac{\int_{-t}^{t} (p - p_0)\,dt}{4\,(q)_{des}\,t}$$

$$+ \frac{b\int_0^1 (P_B - P_0)\,d\frac{x}{b}}{2\,(q)_{des}\,t} \; . \qquad (78)$$

This expression will be used to evaluate the experimental data obtained from the "levapad" test model. These data are shown in Figure 30.

## X. PRESENTATION OF RESULTS

The results of equations (8), (50), and (67) are plotted with the experimentally obtained results (from equation 72) in Figures 21 through 27. Each figure applies to a different model configuration, i.e., a particular centerbody and annular nozzle combination. Experimental results are compared for the three centerbody configurations tested in Figure 28, and for the different $\frac{t}{D_i}$ tested in Figure 29.

Figure 30 pertains to the "levapad" data plotted from equation (78). Experimentally obtained plots of the pressure distribution along the "levapad base" are compared for various $\frac{h}{t}$ tested, in Figure 31. Theoretical (equation 36) and experimentally obtained pressure distribution curves (along the "levapad base") are plotted in Figures 32 through 32b.

These results will be discussed in detail in the section entitled DISCUSSION.

## XI. FLOW VISUALIZATION STUDIES

Visual studies were made of the flow fields for both the annular jet model and the two-dimensional "levapad" model. One-ounce nylon yarn tufts, of approximately $\frac{1}{2}$ inch in length, were affixed to sheets of black painted aluminum (having beveled leading edges), which were placed below the models so that a pictorial representation of the flow could be had. Pictures were taken of these tuft patterns both in and out of ground effect.

The annular jet model, out of ground effect (the "ground plane" completely removed), showed the expected (reference 2) inward turning of the jet (see Figures 15 and 16). This is apparently due to the turbulent expansion of the jet which seals off the base cavity. The entrainment of air from the cavity then tends to create a partial vacuum which in turn tends to pull the jets inward. This surmise was indeed borne out by the slight negative pressures indicated by the manometer board readings. It is interesting to note the upward flow of air at the center of this cavity. This would indicate that a large vortex ring is present at this height (see Figure 15). On reducing the height above the ground plane to two inches ($\frac{h}{D_i} = 0.168$) the tuft picture indicates the presence of a similar though smaller, vortex ring. This correlates with previous investigations of two-dimensional models (references 5 and 8). (See also Figures 17 and 3).

At a height of one inch above the ground plane ($\frac{h}{D_i} = 0.084$)

the tufts appear not to show the vortex structure (Figure 18). However, the tufts do show that a portion of the jet flow is turned inward toward the center of the base. This should dispel the hypothesis that the entire jet follows a smooth "free vortex" curve outward, becoming tangent to the ground without a stagnation point (as reported in reference 2). No upward turning of the tufts was observed at this height and it would appear that as the height is decreased, the base cavity becomes more of a "stagnation" region (see Figure 18).

As the "levapad" height was increased it was interesting to note that a definite (large) symmetrical pair of counter-rotating vortices were apparent (see Figure 19). This was perhaps due in part to the presence of the ground plane which, although it was at a relatively large distance from the jet, still influenced the flow pattern.

In general the flow patterns were as predicted in the literature (references 2 and 8). The one notable discrepancy was the assumption in reference 2 of "ideal" flow (Figure 3).

## XII. DISCUSSION

The theoretical prediction for the augmentation ratio in two-dimensions (equation (50)) is observed to vary considerably from the experimental plots of equation (72) (see Figures 21 through 27). As with the "thin jet" theory, (equation (2)) and practically all other theoretical predictions in the literature, the lift augmentation curves of equation (50) approach a value of infinity as $\frac{h}{D}$ approaches its limit value of zero. This infinity is of course not physically possible and any experimentally obtained augmentation ratio will have some finite upper limit, however large, at the zero-height condition. In the important operating region of $h \leq t$, equation (50) is believed to be an improvement over Pinnes' theory, since his theory is invalid for these heights.

The three-dimensional theory (equation (67)), a semi-empirical adaptation of equation (50), is believed to be in reasonable accord with experiment (see Figures 21 through 27). A plot of equation (67) will approach some finite value of augmentation ratio as the height approaches zero.

The experimental augmentation ratios for this thesis are slightly higher, in general, for centerbody "B" than they are for centerbody "A" for a given nozzle thickness (see Figure 28). The test performed with no centerbody, and with a nozzle thickness of 0.375 inches, ($\frac{t}{D_i} = 0.032$), shows a still higher value of augmentation ratio than did the tests with either centerbody "A" or

centerbody "B", for the same nozzle thickness. It would thus appear that a centerbody is not necessary, and indeed, may even decrease performance.

Of more significance was the difference in magnitude of augmentation ratios obtained by varying the nozzle thickness. Not only did the experimental curves agree more closely with theoretical predictions as the nozzle thickness was decreased, but they were of consistently higher magnitude (see Figure 29). It is therefore quite obvious that proper model design is very important to the attainment of a maximum operating efficiency. By the simple artifice of using the "proper" centerbody geometry and nozzle thickness, the designer can attain a marked increase in the performance of his machine at relatively no "cost" in power input. This point was readily apparent and graphically illustrated while the testing was actually in progress. While the "no centerbody" experiment was being performed, it was found necessary to substantially reduce the air flow rate (in the feed line) in order to maintain the constant pressure ratio at the inlet nozzle (relative to the other model configurations). Had the air flow rate been maintained at a constant value for all model configurations tested, it is believed that the "no centerbody" configuration would have resulted in a markedly higher augmentation ratio than did the others tested.

All tests were performed at a constant ratio of total pressure in the inlet nozzle to atmospheric pressure. This was done to simulate the performance of an actual ground effect machine which would be powered by a "fan." As the machine approaches the ground

the total pressure in the annular nozzle builds up. In the test model the entire system will approach the full total pressure available from the shop air supply as $\frac{h}{D}$ approaches zero. However, in the actual ground effect machine the back pressure would tend to stall the fan as the height is decreased. Therefore, the assumption of a constant pressure ratio throughout all operating heights is made as a rough approximation to the actual fan characteristics.

The two experiments performed on the two-dimensional "levapad" model resulted in almost identical augmentation ratio curves for each of the two nozzles tested but with the curve for the thinner (0.625 inch) nozzle being slightly higher in magnitude than that for the 1.70 inch nozzle. Both curves were of appreciably lower magnitude than were those of any of the axi-symmetric model configurations tested. This may be due to the lack of a pressure "bubble," such as exists under the base of the annular jet. The most noteworthy aspect of the "levapad" testing was the comparison of input air flow rates for the two nozzles. The thinner nozzle (0.625 inches, $\frac{t}{b} = 0.025$) required considerably less air flow to maintain a constant inlet nozzle pressure ratio than did the wider nozzle (1.70 inches, $\frac{t}{b} = 0.067$) to maintain the same pressure ratio. The significance of this has been discussed previously in this section. It is believed that the very thin nozzle will allow a much higher pressure ratio to be maintained at the inlet nozzle, and would probably allow higher augmentation ratios to be maintained for a given air flow rate.

The pressure distribution on the "levapad base" was plotted for various $\frac{h}{t}$ ratios tested (Figures 32 through 32b). The theoretical pressure distributions obtained from equation (36) for the same $\frac{h}{t}$ were also plotted in these figures for comparison with experiment. The "exact" theoretical curves are seen to approach negative infinity at the corner "E", and zero at point "A,F" (see Figure 4a) for all $\frac{h}{t}$. The experimental curves are observed to correspond more closely with theory as $\frac{h}{t}$ increases, i.e., as the "levapad" moves toward the out of "ground effect" positions. Five experimentally obtained pressure distribution curves were plotted for various $\frac{h}{t}$ (Figure 31), for comparative purposes. It is believed that the effect of viscosity is one of the predominant factors causing the increased deviation between the theory and experiment as $\frac{h}{t}$ decreases.

## XIII. CONCLUSIONS AND RECOMMENDATIONS

As a result of evaluating the material contained in this thesis the following conclusions and recommendations are submitted:

A. Conclusions

1. It is believed that the theory developed in this thesis is an improvement over current "thick jet" theories in the operating region for $h \leq t$. It is noted that appreciable variations in magnitude of augmentation ratios can be obtained by varying the model geometry. However, it is felt that it would be practically impossible to derive a theoretical expression for augmentation ratio as a function of centerbody geometry.

2. As noted above, internal model geometry is an important factor in obtaining maximum performance. Certainly there is some optimum combination of centerbody design and annular nozzle design that will enable the designer to obtain maximum operating efficiency (over an established range of $\frac{h}{D}$ values).

3. It is believed that jet entrainment and mixing effects may be appreciable in the "ground effect" operating region. Flow visualization studies

indicate that Chaplin's assumption of an "ideal" jet is not a valid approximation. The vortex pattern indicates that a considerable amount of air is entrained from the cavity and then "fed" back into it.

4. While the theory developed in this thesis is believed to be a valid approximation, it is limited in accuracy (as are all known previous theories) by the basic assumption of inviscid flow. The Schwarz-Christoffel transform is probably as strong a tool as the aerodynamicist has at his disposal, within its basic assumptions. However, it is believed that the effect of viscosity may be a consideration of paramount importance.

5. By keeping a constant total pressure ratio in the inlet nozzle, as suggested in the literature, it is believed that a reasonable approximation to the operation of an actual ground effect machine can be obtained. This approximation is based on a machine which is powered by a power driven "fan."

B. Recommendations

1. It is recommended that any further testing of annular jet models include a "no-centerbody"

configuration, i.e., with nothing but a flat base plate in the center of the machine. Any centerbody configurations tested should be designed so as to fill as small a space as possible in the interior chamber (perhaps similar to centerbody "B", but considerably thinner). It is believed that such a configuration may offer the most efficient performance.

2. Similarly, annular nozzle openings should be kept relatively thin ($\frac{t}{D_i} \leq 0.030$), again to increase performance.

3. Any further theoretical flow analyses should include the effects of viscosity and mixing when-and where-ever possible. If this is found to be impractical, it is recommended that extensive experimentation be performed, varying as many parameters as possible. If enough empirical data can be collected and catalogued, criteria can be established for obtaining maximum performance of these machine types.

## XIV. ACKNOWLEDGEMENTS

The most sincere appreciation of the author is expressed to Dr. Robert W. Truitt, Dr. James B. Eades, Jr., and Prof. Arthur C. Bruce for their valuable opinions and advice.

The author also wishes to express his appreciation to , for his very able assistance in the design and construction of the annular jet test stand.

## XV. BIBLIOGRAPHY

1. Boehler, G. D., Ground Effect Machines. Aircraft Engineering, May 1960.

2. Chaplin, H. R., Theory of the Annular Nozzle in Proximity to the Ground. David Taylor Model Basin, Aero Report 923, July, 1957.

3. Chaplin, H. R., and Stephenson, B., Preliminary Study of the Hovering Performance of Annular Jet Vehicles in Proximity to the Ground. David Taylor Model Basin, Aero Report 947, August, 1958.

4. Milne-Thomson, L. M., Theoretical Hydrodynamics. London, 1938.

5. Nixon, W. B., and Sweeney, T. G., Preliminary Flight Experiments with the Princeton University 20-Ft Ground Effect Machine. Aero/Space Engineering, April, 1960.

6. Pinnes, R. W., A Power Plant Man's Look at the Ground Effect Machine. Journal of the American Helicopter Society, July, 1959.

7. Pinnes, R. W., The Propulsion Aspects of Ground Effect Machines. I.A.S. Paper No. 60-13.

8. Proceedings of the Symposium of Ground Effect Phenomena, presented at the Princeton University Conference. October 21-23, 1959.

9. von Glahn, U. H., Exploratory Study of Ground Proximity Effects on Thrust of Annular and Circular Nozzles. NACA TN 3982, April, 1957.

The two page vita has been removed from the scanned document. Page 1 of 2

The two page vita has been removed from the scanned document. Page 2 of 2

TABLE I

COMPARISON OF VALUES OBTAINED FOR LIFT AUGMENTATION RATIO OF THE ANNULAR JET

| Model Configuration | | | | Experimental Augmentation Ratios | | | Theoretical Augmentation Ratios | |
|---|---|---|---|---|---|---|---|---|
| t (in) | h (in) | $\frac{h}{D_i}$ or $\frac{h}{b}$ | $\frac{t}{D_i}$ or $\frac{t}{b}$ | Centerbody "A" | Centerbody "B" | No Centerbody | Two-Dimensional | Three-Dimensional |
| 0.075 | 0.125 | 0.011 | 0.006 | 58.17 | 41.08 | | 7.00 | 50.00 |
| 0.075 | 0.250 | 0.021 | 0.006 | 45.80 | 33.56 | | | |
| 0.075 | 0.375 | 0.032 | 0.006 | 40.04 | 28.63 | | | |
| 0.075 | 0.500 | 0.042 | 0.006 | 31.67 | 23.98 | | | |
| 0.075 | 0.625 | 0.053 | 0.006 | 25.79 | 19.35 | | | |
| 0.075 | 0.750 | 0.063 | 0.006 | 19.99 | 16.08 | | | |
| 0.075 | 0.875 | 0.074 | 0.006 | 15.96 | 13.56 | | | |
| 0.075 | 1.000 | 0.084 | 0.006 | 13.24 | 11.33 | | | |
| 0.375 | 0.125 | 0.011 | 0.032 | 22.42 | 25.12 | 27.90 | | 18.00 |
| 0.375 | 0.250 | 0.021 | 0.032 | 16.73 | 16.53 | 19.50 | 18.00 | 16.05 |
| 0.375 | 0.375 | 0.032 | 0.032 | 14.48 | 13.86 | 15.20 | 7.00 | 14.30 |
| 0.375 | 0.500 | 0.042 | 0.032 | 13.04 | 12.23 | 14.30 | 3.80 | 13.10 |
| 0.375 | 0.625 | 0.053 | 0.032 | 12.18 | 11.20 | 13.00 | 2.20 | 12.25 |
| 0.375 | 0.750 | 0.063 | 0.032 | 10.99 | 10.16 | 11.60 | 1.20 | 11.30 |
| 0.375 | 0.875 | 0.074 | 0.032 | 10.16 | 9.77 | 10.60 | 1.00 | 10.95 |
| 0.375 | 1.000 | 0.084 | 0.032 | 9.52 | 9.26 | 9.40 | 0.80 | 10.40 |
| 0.625 | 0.125 | 0.011 | 0.053 | 9.24 | 20.51 | | | 7.75 |
| 0.625 | 0.250 | 0.021 | 0.053 | 7.99 | 11.90 | | 25.00 | 7.15 |
| 0.625 | 0.375 | 0.032 | 0.053 | 7.02 | 8.94 | | 16.20 | 6.90 |
| 0.625 | 0.500 | 0.042 | 0.053 | 6.29 | 8.05 | | 9.00 | 6.20 |
| 0.625 | 0.625 | 0.053 | 0.053 | 5.96 | 7.78 | | 5.00 | 6.00 |
| 0.625 | 0.750 | 0.063 | 0.053 | 5.59 | 7.22 | | 3.50 | 5.70 |
| 0.625 | 0.875 | 0.074 | 0.053 | 5.39 | 7.02 | | 2.50 | 5.45 |
| 0.625 | 1.000 | 0.084 | 0.053 | 5.24 | 6.66 | | 1.80 | 5.30 |

TABLE II

COMPARISON OF VALUES OF LIFT AUGMENTATION RATIO FOR THE "LEVAPAD"

| "Levapad" Model Configuration | | | | Experimental Augmentation Ratios |
|---|---|---|---|---|
| t (in) | h (in) | $\frac{h}{b}$ | $\frac{t}{b}$ | |
| 1.70 | 0.125 | 0.010 | 0.135 | 1.40 |
| 1.70 | 0.250 | 0.021 | 0.135 | 1.01 |
| 1.70 | 0.375 | 0.031 | 0.135 | 0.88 |
| 1.70 | 0.500 | 0.041 | 0.135 | 0.77 |
| 1.70 | 0.625 | 0.052 | 0.135 | 0.72 |
| 1.70 | 0.750 | 0.062 | 0.135 | 0.69 |
| 0.625 | 0.125 | 0.010 | 0.049 | 1.49 |
| 0.625 | 0.250 | 0.021 | 0.049 | 1.26 |
| 0.625 | 0.375 | 0.031 | 0.049 | 1.09 |
| 0.625 | 0.500 | 0.041 | 0.049 | 1.02 |
| 0.625 | 0.625 | 0.052 | 0.049 | 0.95 |
| 0.625 | 0.750 | 0.062 | 0.049 | 0.90 |

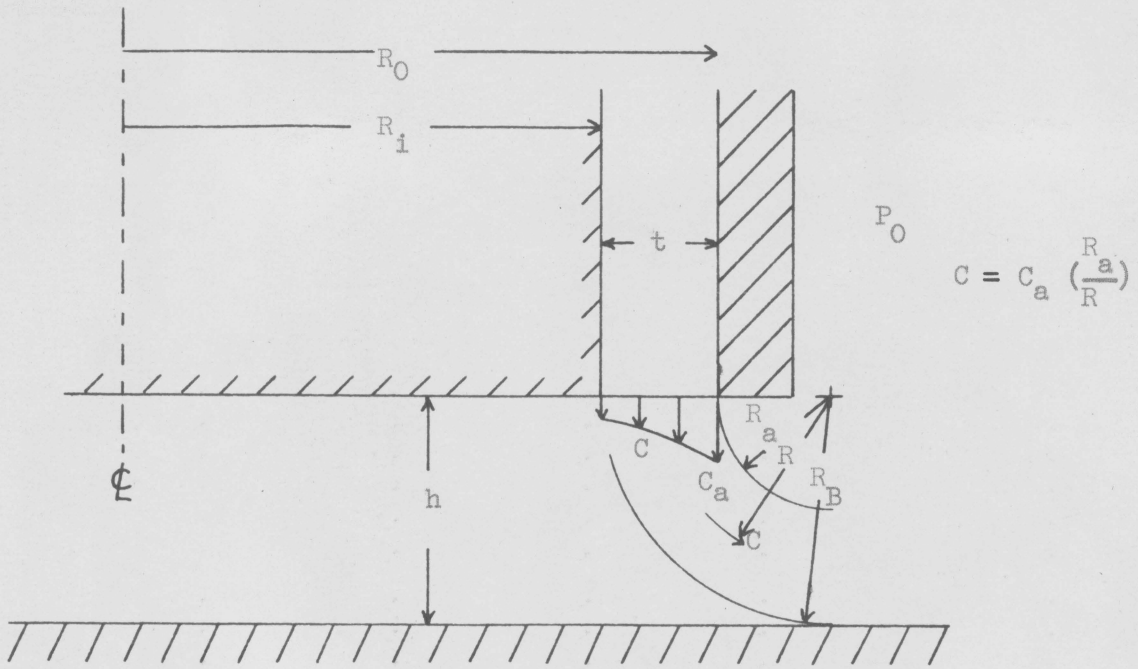


MERIDIONAL PLANE ANNULAR JET NOMENCLATURE

(AFTER PINNES, REFERENCE 6)

FIGURE 1

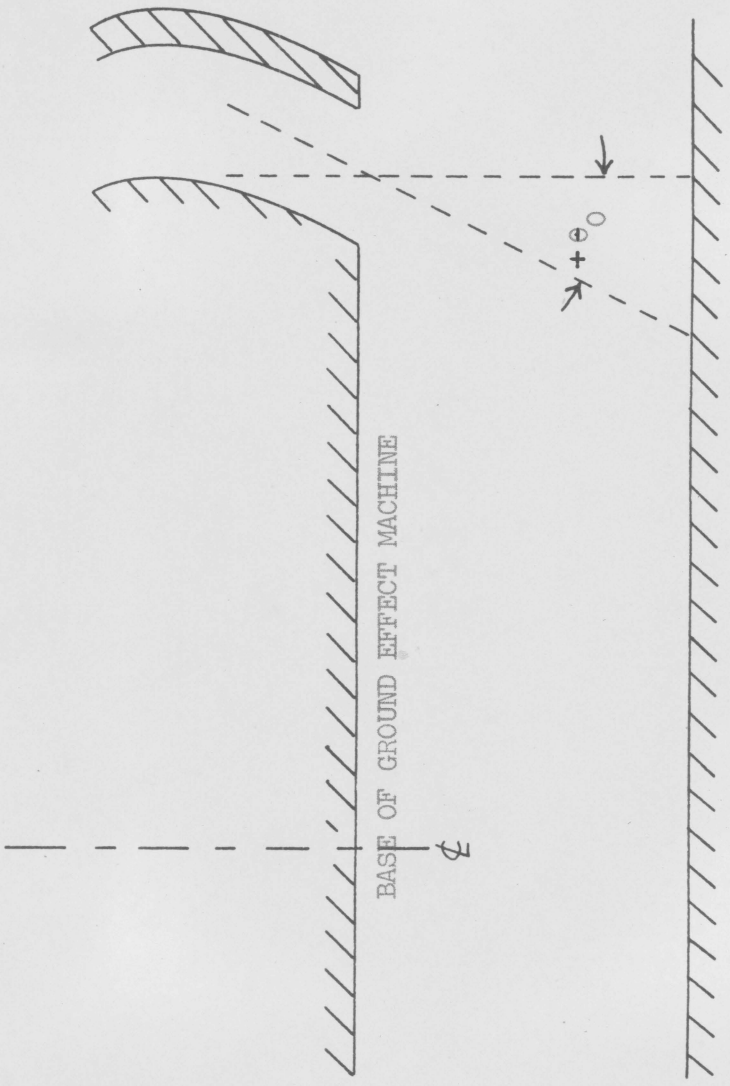


ANNULAR JET NOMENCLATURE (DEFINITION OF $\theta_o$)

FIGURE 1a

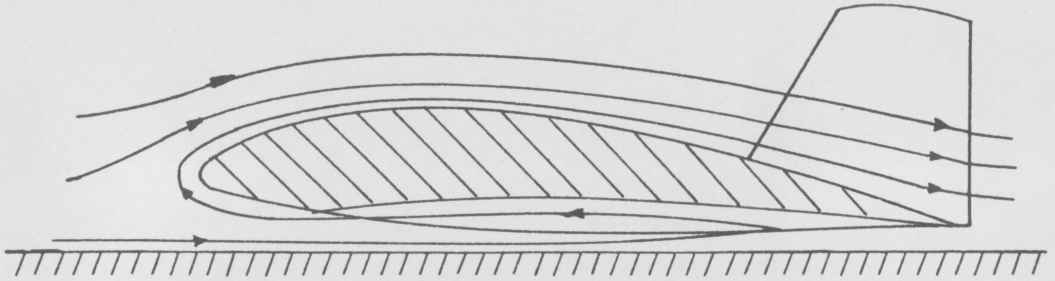

THE RAM WING



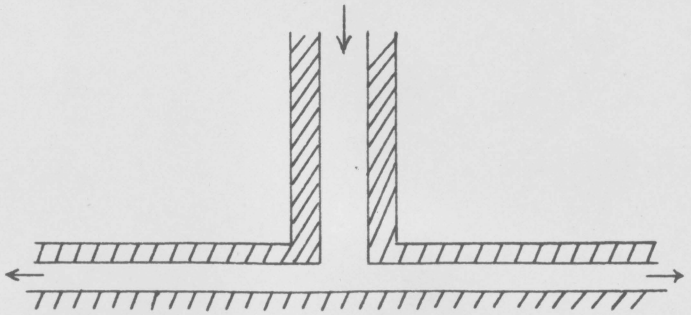

A SIMPLE LEVAPAD

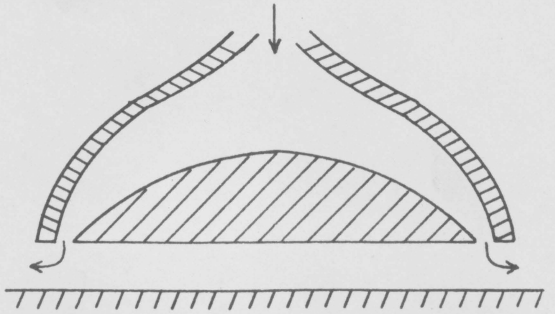

A SIMPLE PERIPHERAL (ANNULAR) JET

THREE DISTINCTIVE TYPES OF GROUND EFFECT MACHINES

FIGURE 2

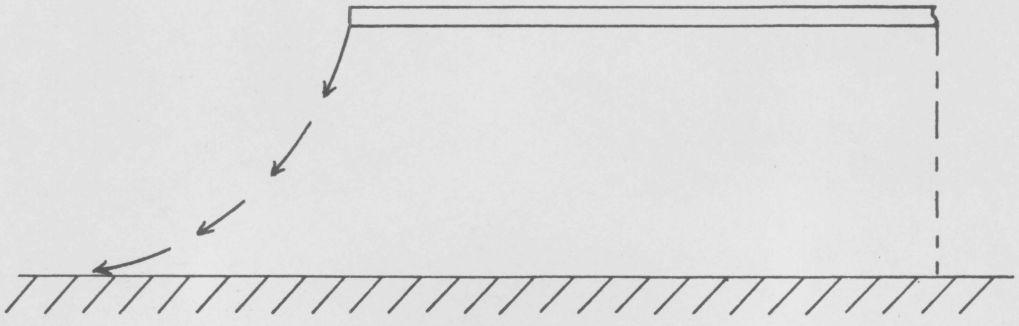

IDEAL FLOW

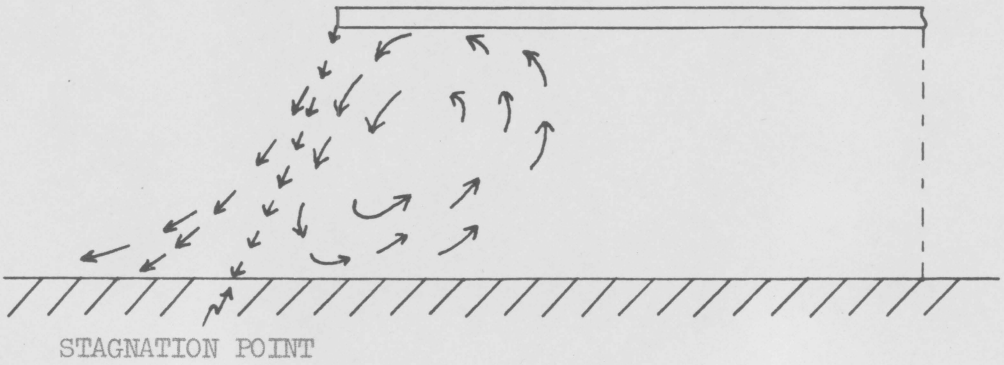


REAL FLOW

COMPARISON OF REAL FLOW AND IDEAL FLOW IN

THE ANNULAR JET

FIGURE 3

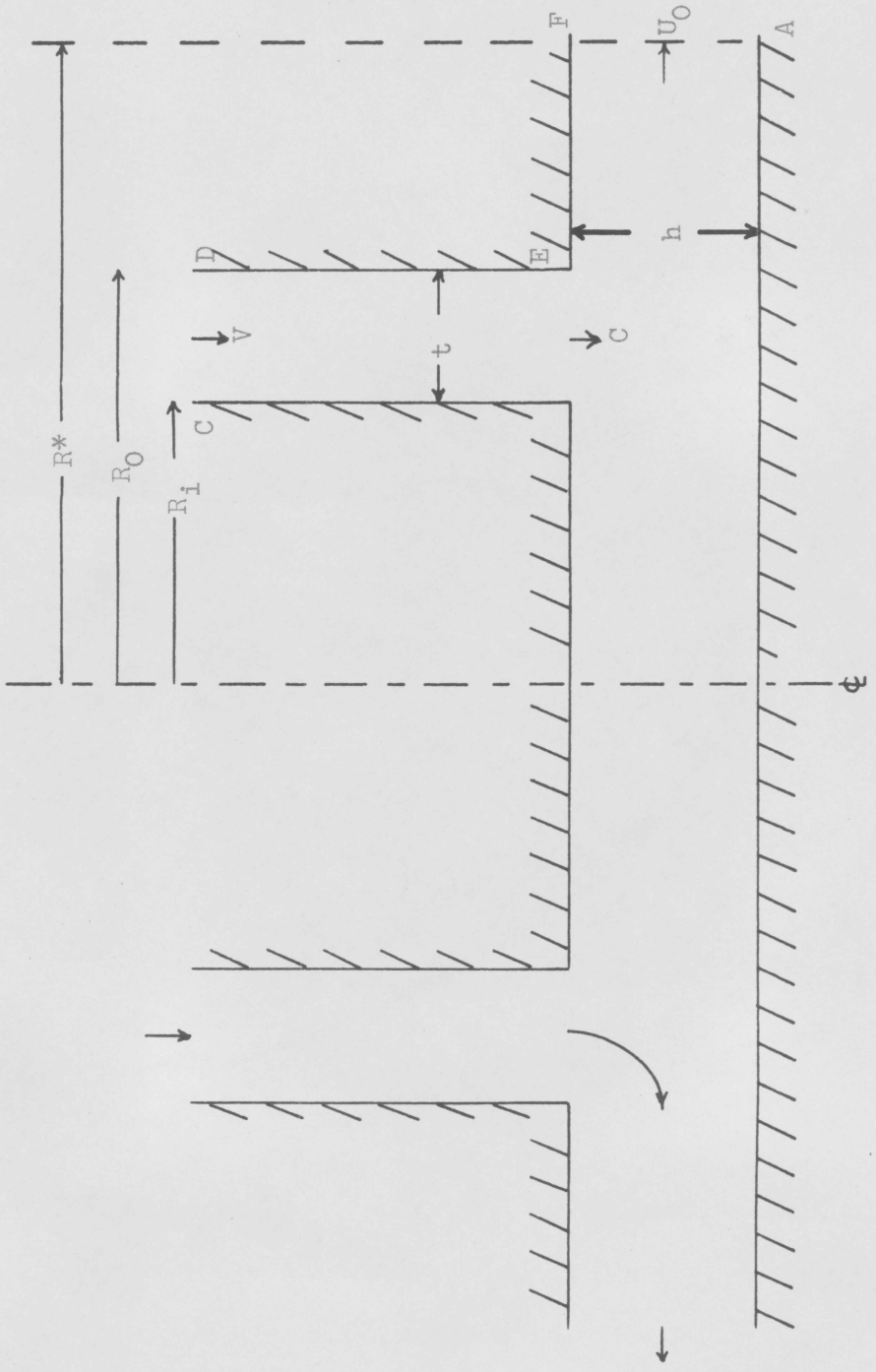


SCHEMATIC TWO-DIMENSIONAL CROSS SECTION OF FLOW FROM AN ANNULAR JET

FIGURE 4

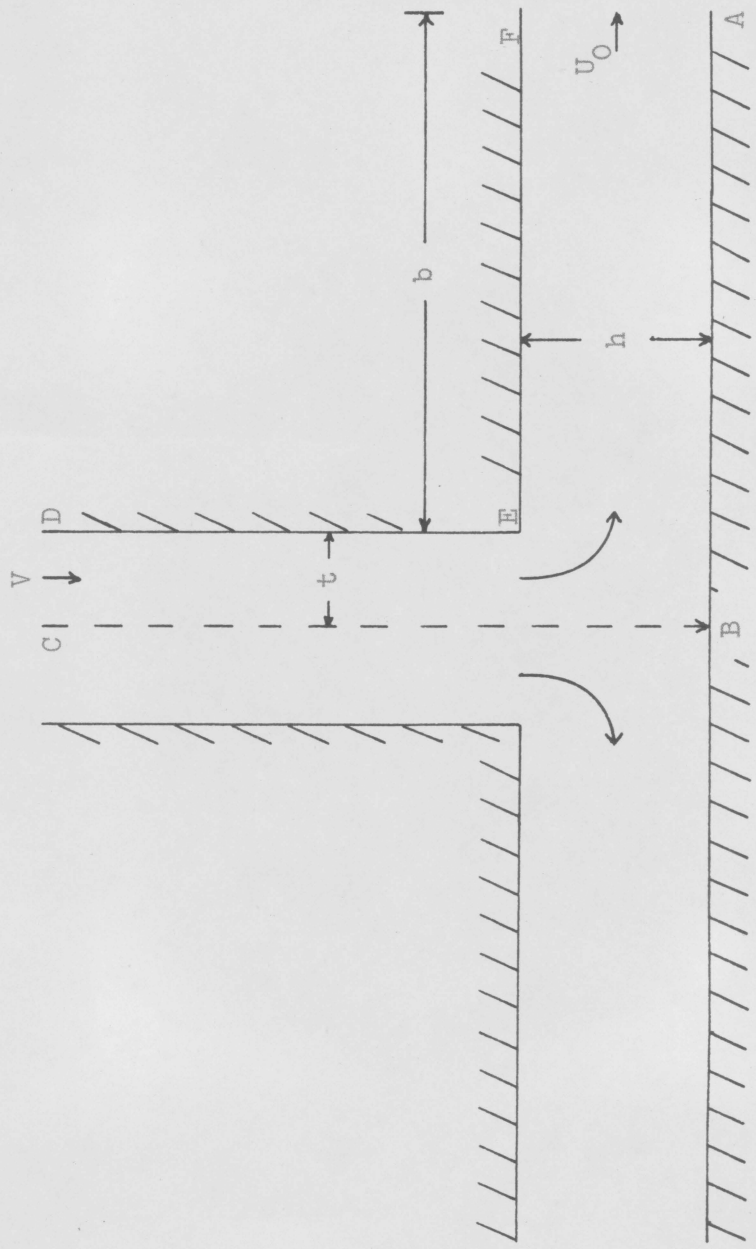


LEVAPAD DIAGRAM SHOWING DIVIDING STREAMLINE BC AND NOMENCLATURE

FIGURE 4a

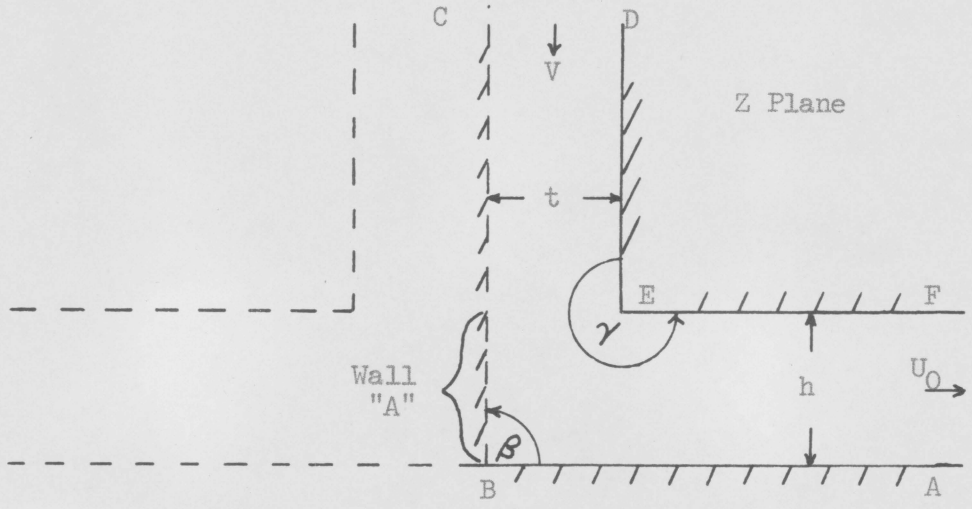


"LEVAPAD" DIAGRAM MODIFIED TO APPROXIMATE A TWO-DIMENSIONAL CROSS SECTIONAL VIEW OF FLOW FROM ONE HALF OF AN ANNULAR JET IN GROUND EFFECT (" Z" PLANE OF SCHWARZ-CHRISTOFFEL TRANSFORM)

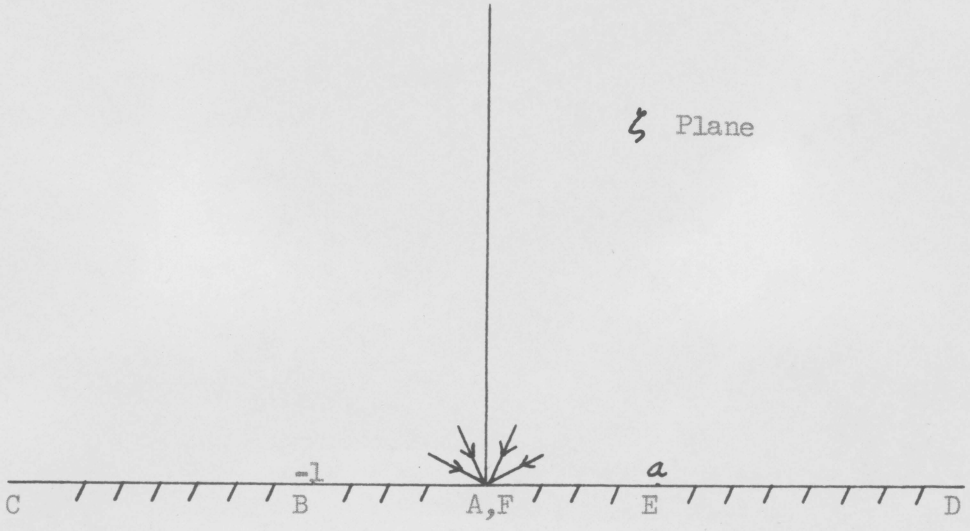


MAPPING OF ABOVE DIAGRAM ON "ζ" PLANE

FIGURE 4b

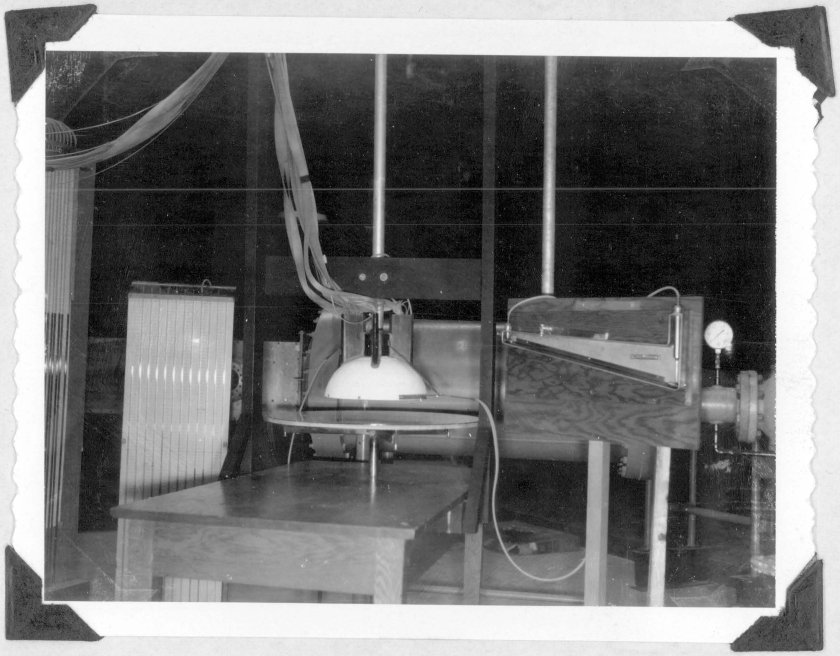

THREE-DIMENSIONAL ANNULAR JET TEST STAND

FIGURE 5

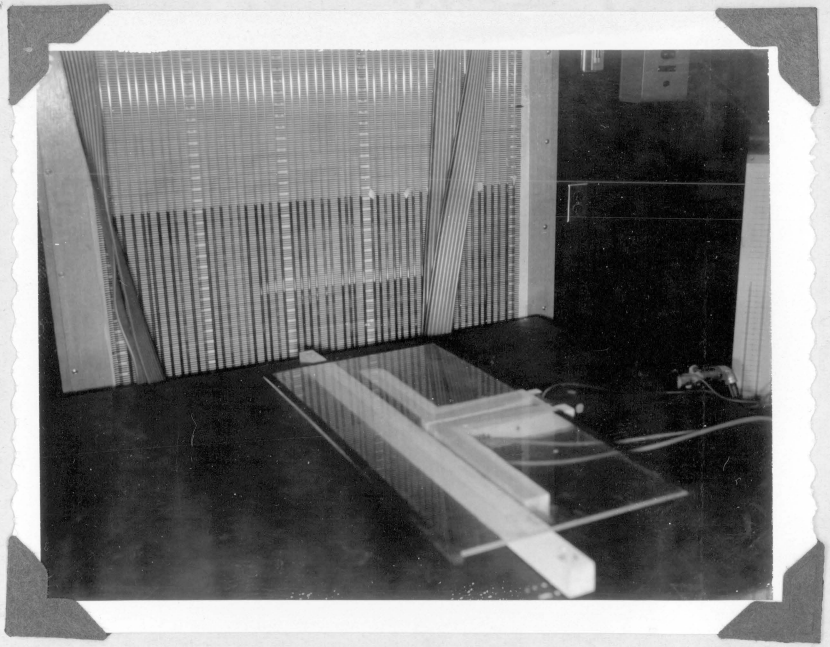

TWO-DIMENSIONAL "LEVAPAD" TEST APPARATUS

FIGURE 6

VIEW OF CENTERBODY "A" SHOWING BALSA VANES

FIGURE 7

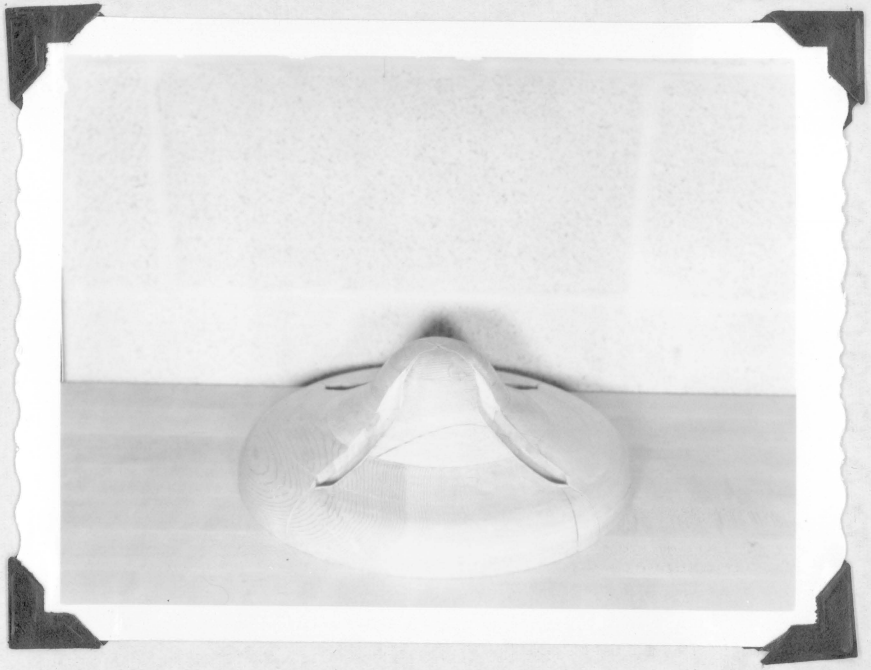

CENTERBODY "B" SHOWING CUT-OUT ALLOWING FOR PASSAGE

OF PRESSURE LINE SUPPORT VANES

FIGURE 8

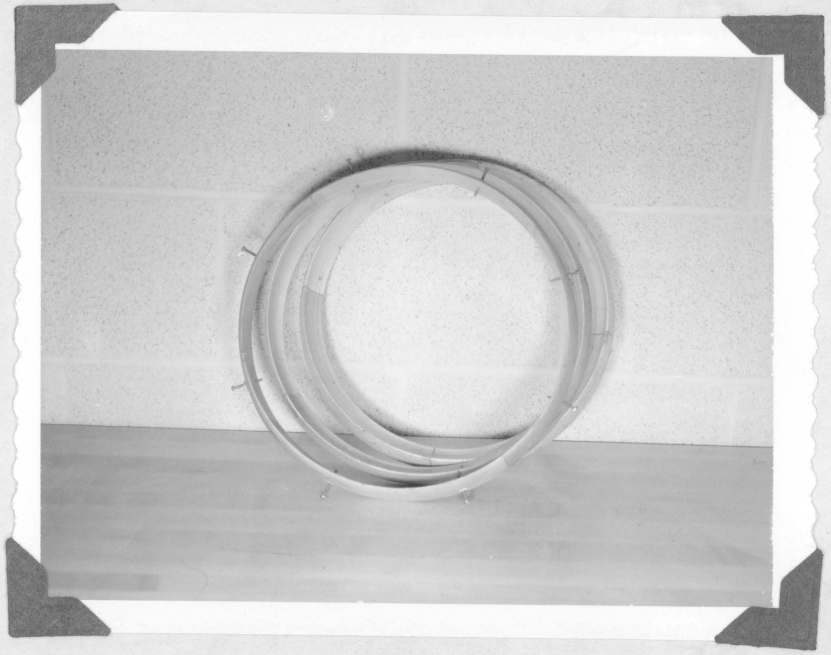

INTERCHANGEABLE ANNULAR NOZZLE RINGS

FIGURE 9

ANNULAR NOZZLE RING

FIGURE 10

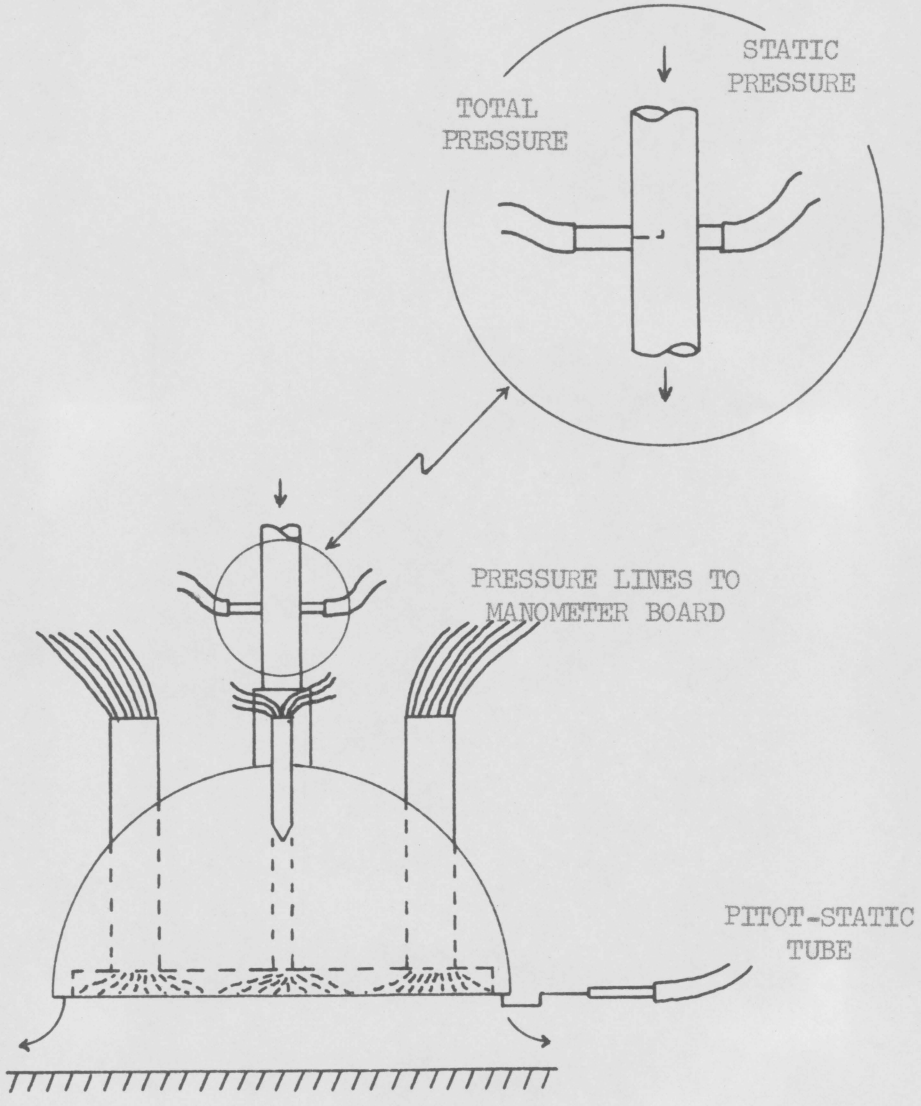


SCHEMATIC DRAWING SHOWING INSTRUMENTATION OF

ANNULAR JET MODEL

FIGURE 11

PITOT-STATIC TUBE USED IN THREE-DIMENSIONAL ANNULAR JET

FIGURE 12

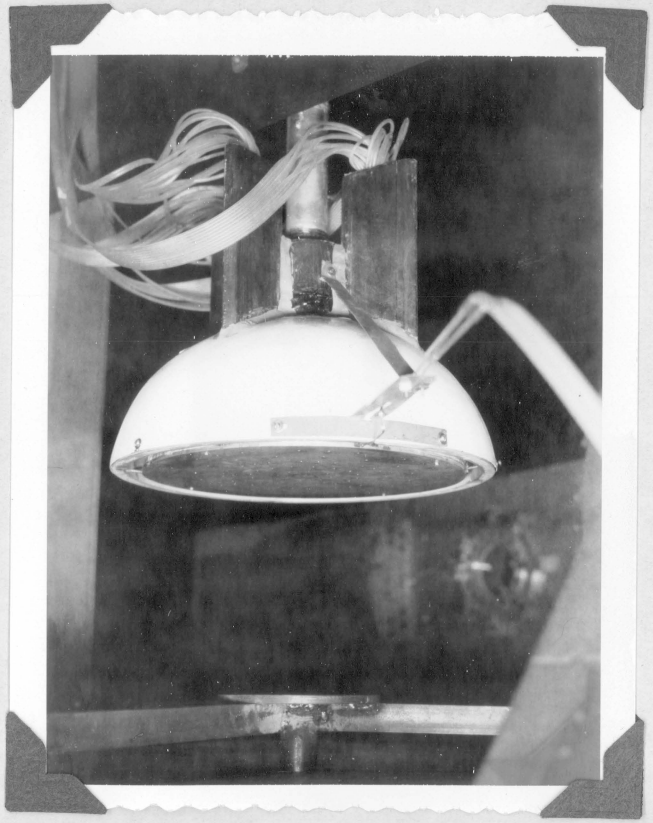

BOTTOM VIEW OF ANNULAR JET MODEL, SHOWING BASE PLATE PRESSURE TAPS AND PITOT-STATIC TUBE ARRANGEMENT

FIGURE 13

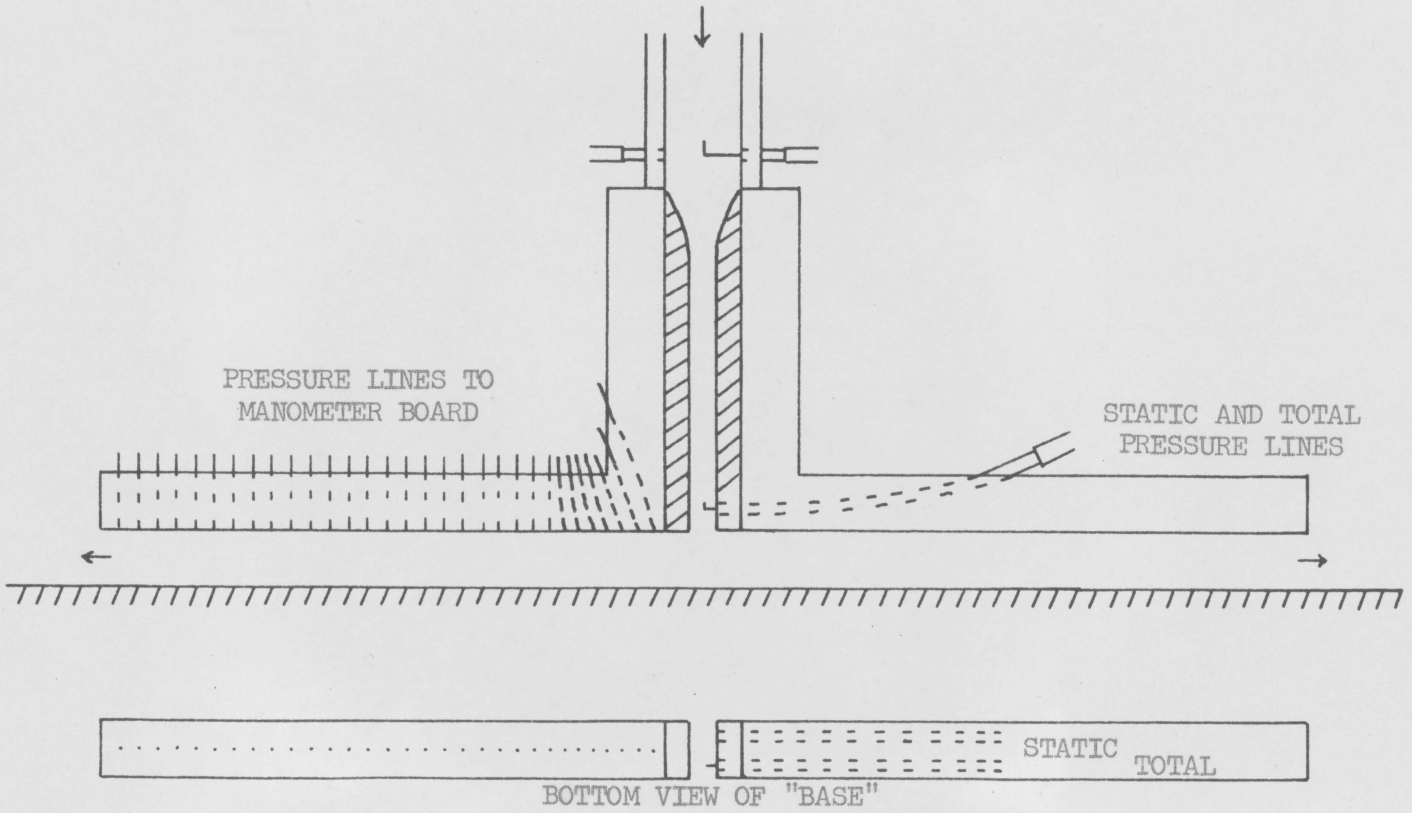


SCHEMATIC DRAWING OF "LEVAPAD" TEST STAND SHOWING INSTRUMENTATION

$(\frac{t}{b} = 0.025)$

FIGURE 14

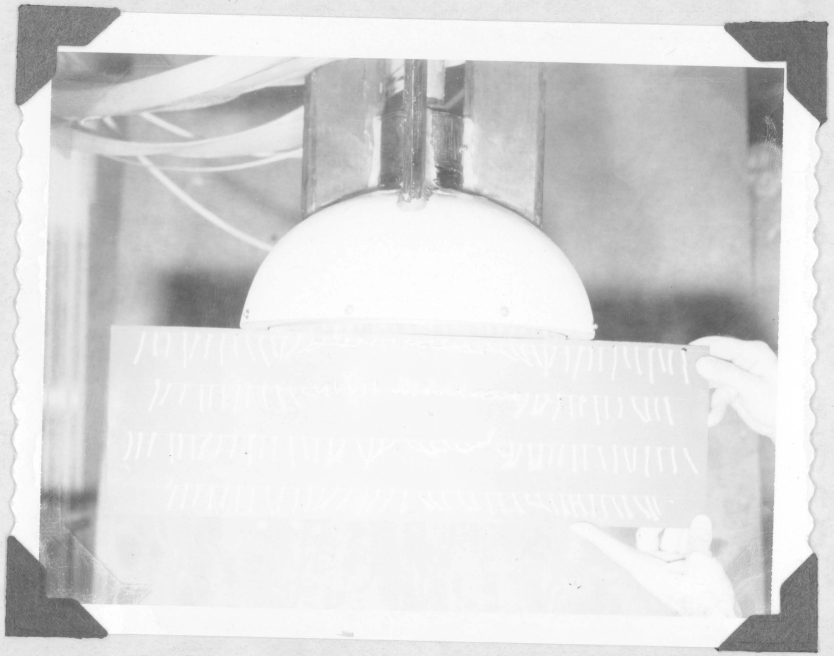

ANNULAR JET TUFT PATTERN OUT OF "GROUND EFFECT"

FIGURE 15

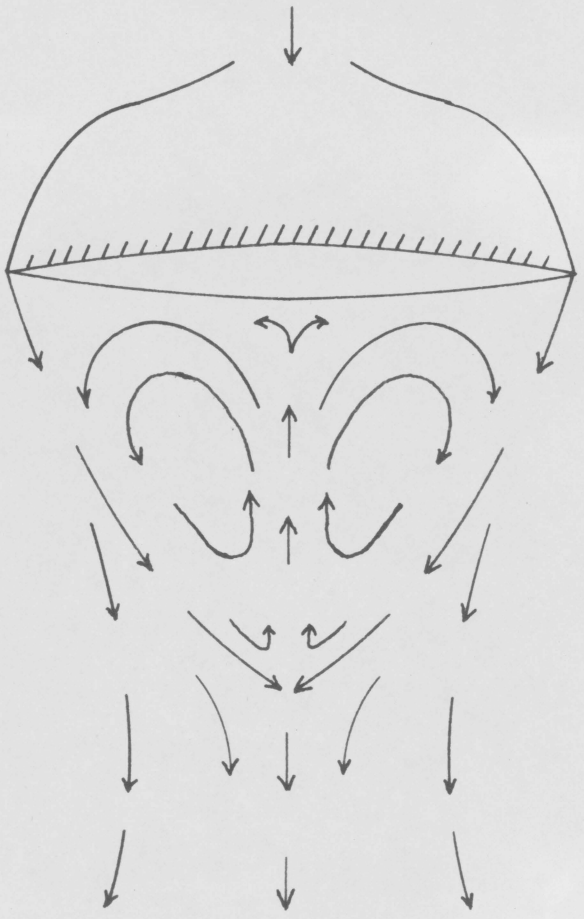

IDEAL FLOW FIELD FOR THE ANNULAR NOZZLE AT HIGH ALTITUDE (AFTER CHAPLIN, REFERENCE 2)

FIGURE 16

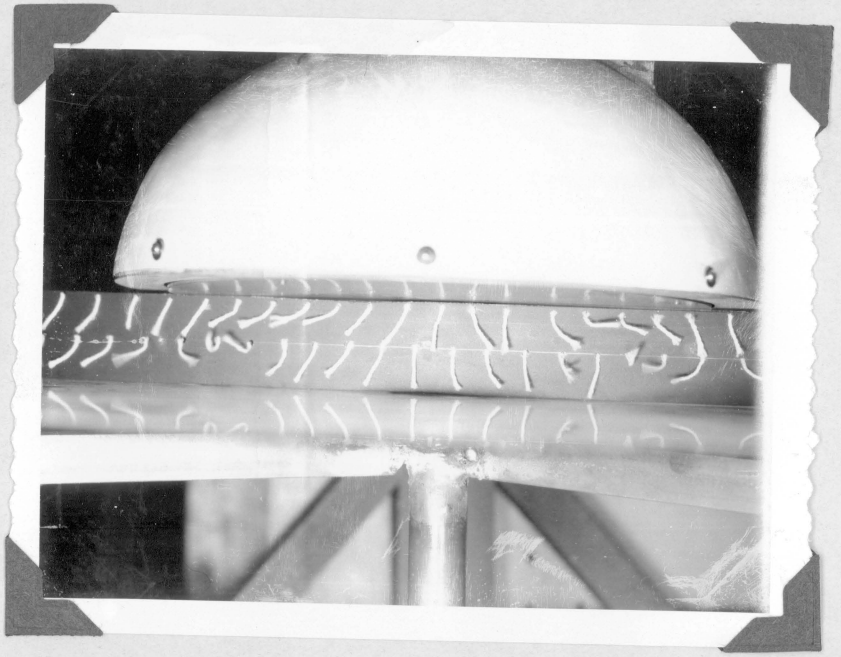

ANNULAR JET IN "GROUND EFFECT"

$(\frac{h}{D_1} = 0.168)$

FIGURE 17

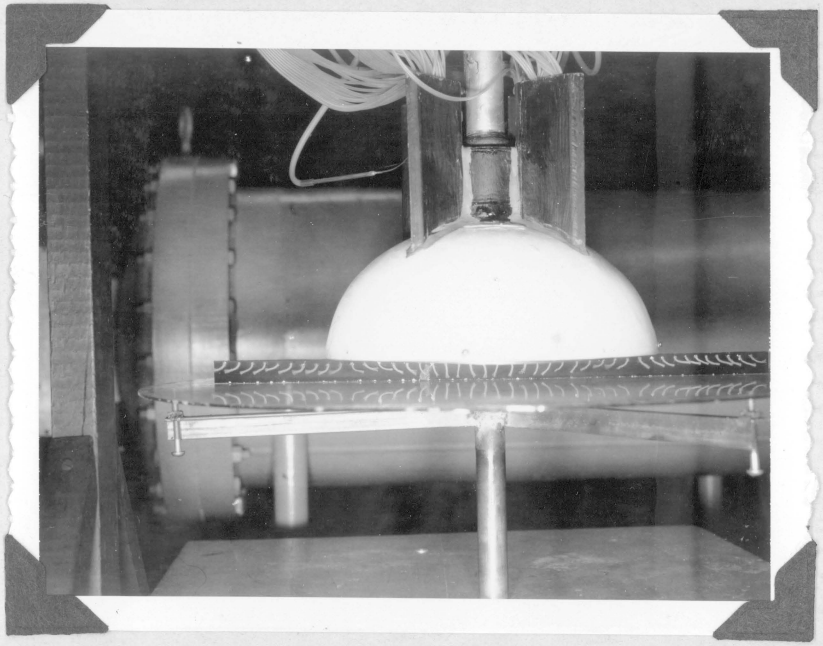

ANNULAR JET IN "GROUND EFFECT"

$(\frac{h}{D_i} = 0.084)$

FIGURE 18

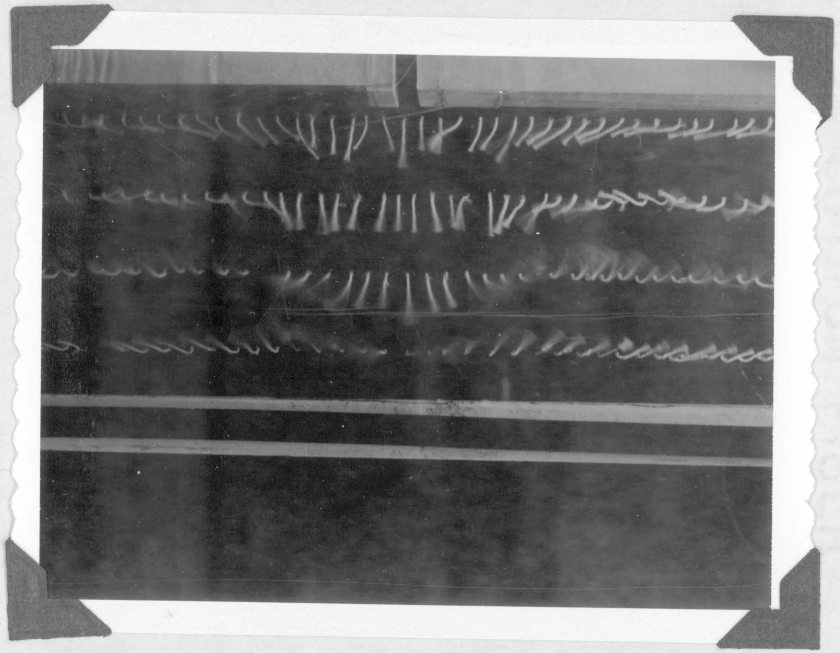

"LEVAPAD" OUT OF "GROUND EFFECT"

FIGURE 19

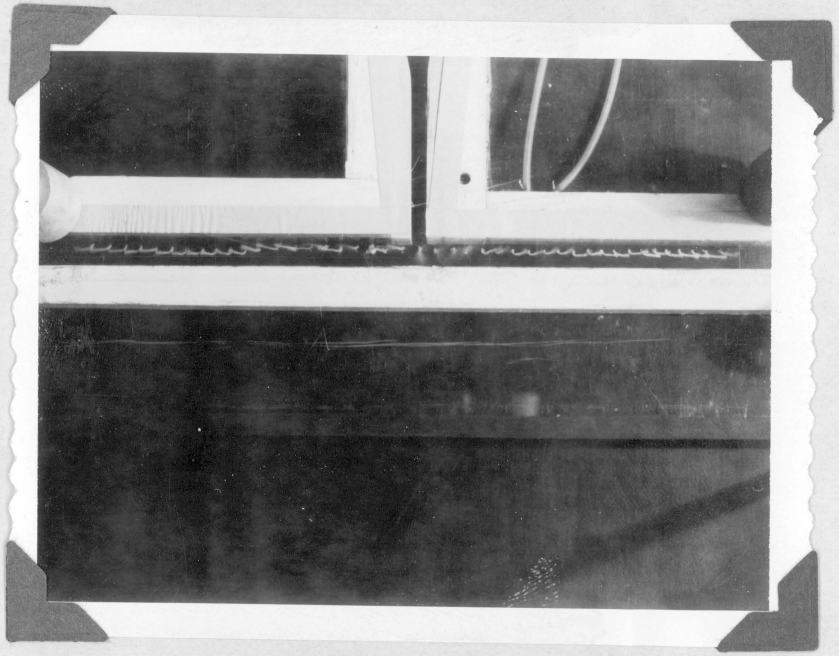

"LEVAPAD" IN "GROUND EFFECT"

$\frac{t}{b} = 0.049$

FIGURE 20

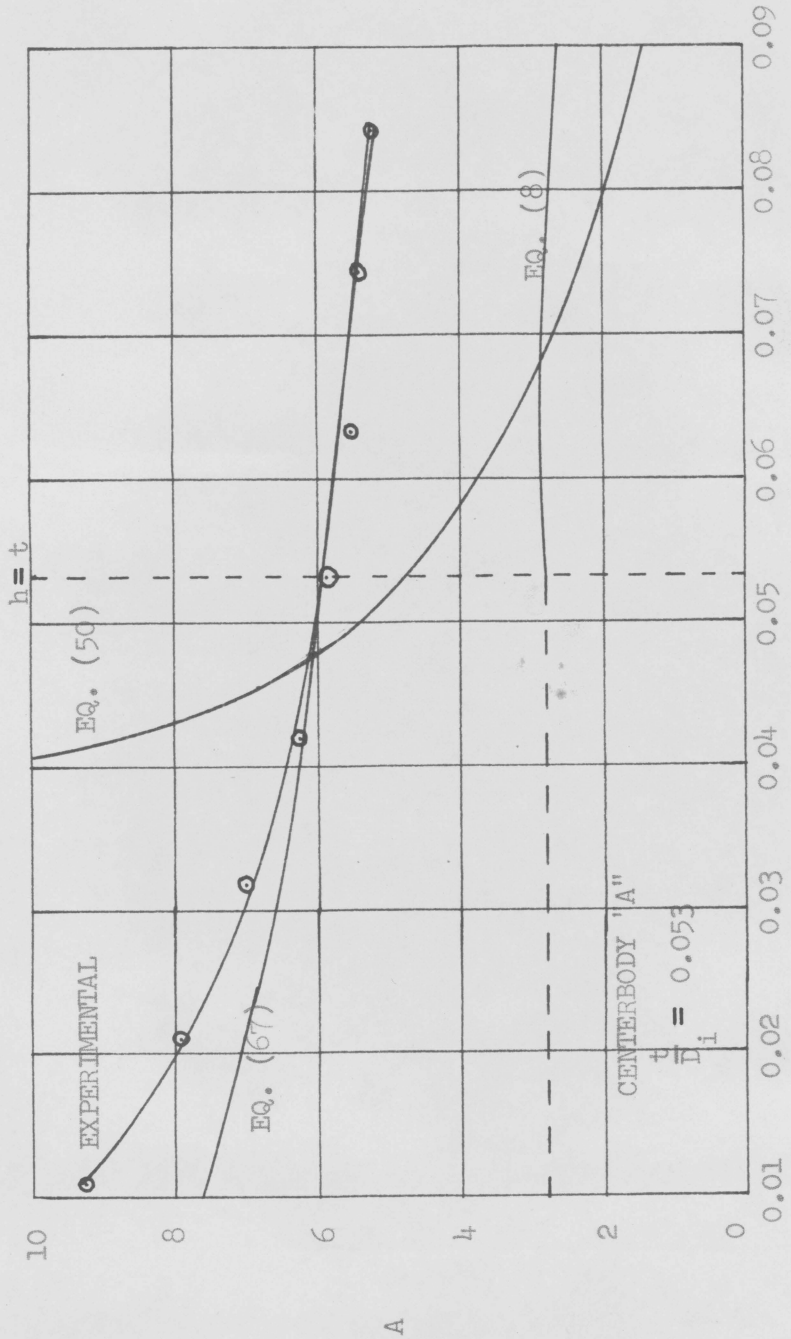


LIFT AUGMENTATION RATIO VERSUS $\frac{h}{D_i}$ (or $\frac{h}{b}$)

FIGURE 21

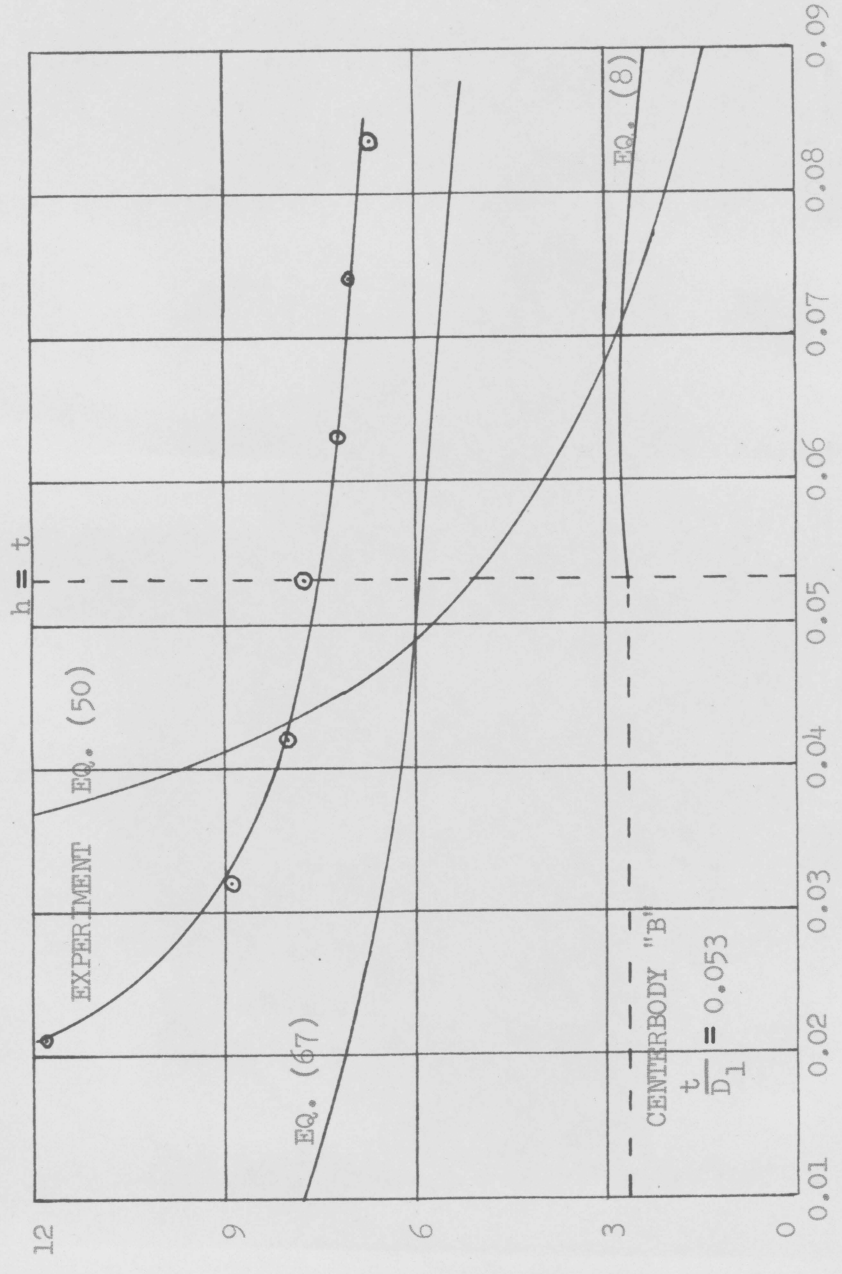


LIFT AUGMENTATION RATIO VERSUS $\frac{h}{D_i}$ (or $\frac{h}{b}$)

FIGURE 22

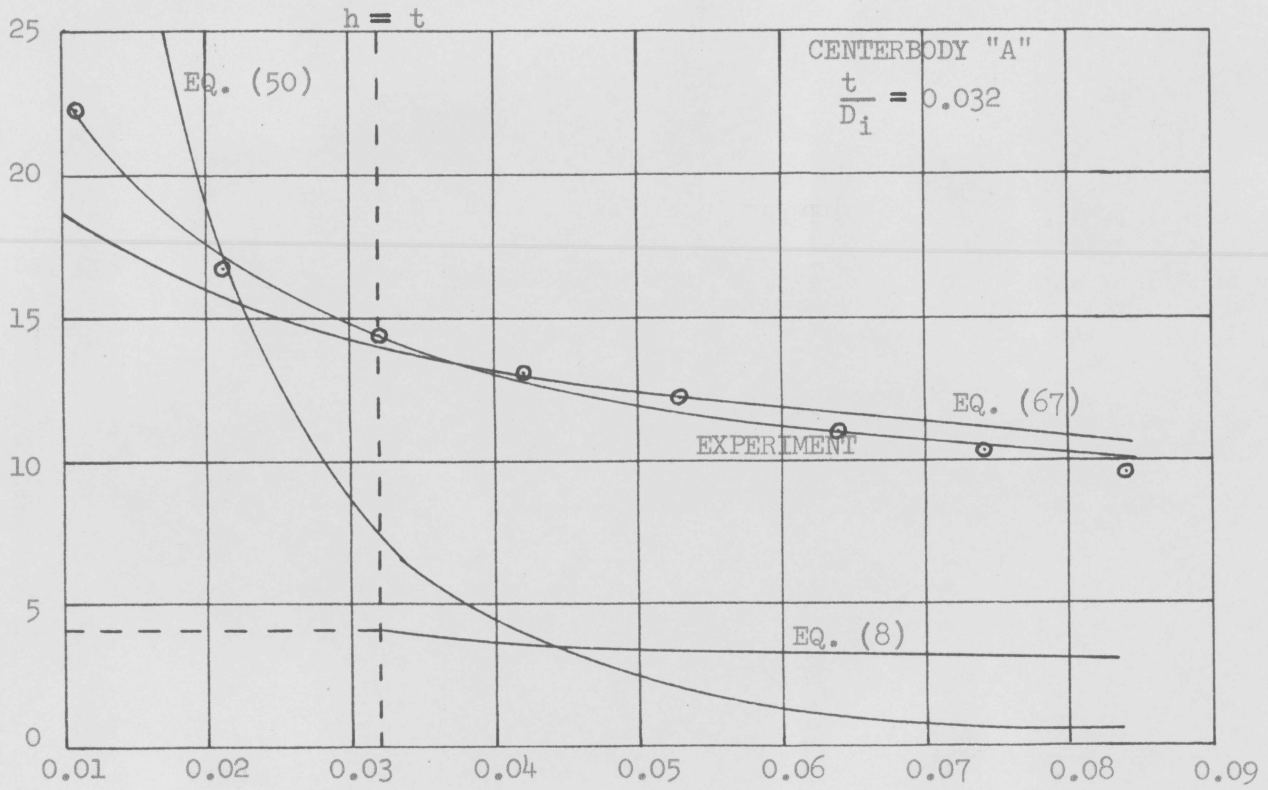


LIFT AUGMENTATION RATIO VERSUS $\frac{h}{D_i}$ (or $\frac{h}{b}$)

FIGURE 23

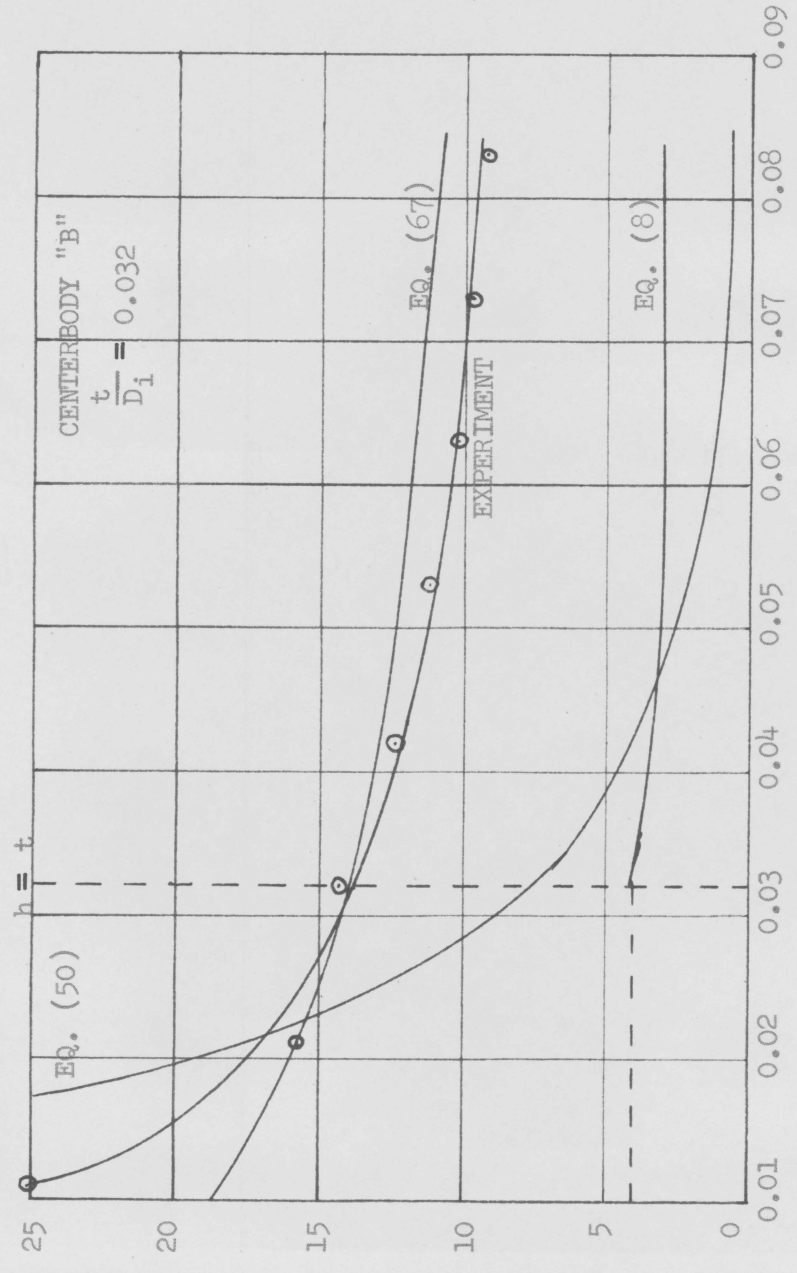


LIFT AUGMENTATION RATIO VERSUS $\frac{h}{D_i}$ (or $\frac{h}{b}$)

FIGURE 24

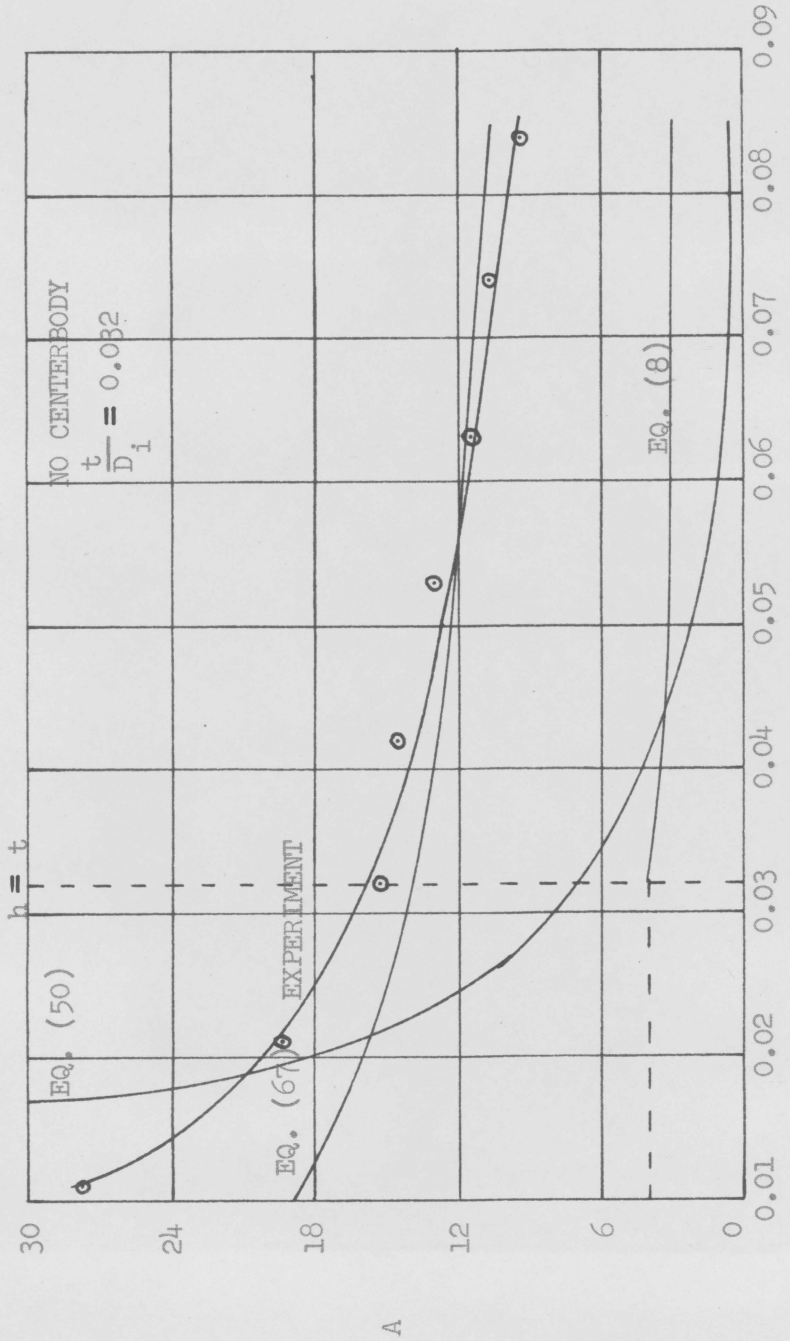


LIFT AUGMENTATION RATIO VERSUS $\frac{h}{D_i}$ (or $\frac{h}{b}$)

FIGURE 25

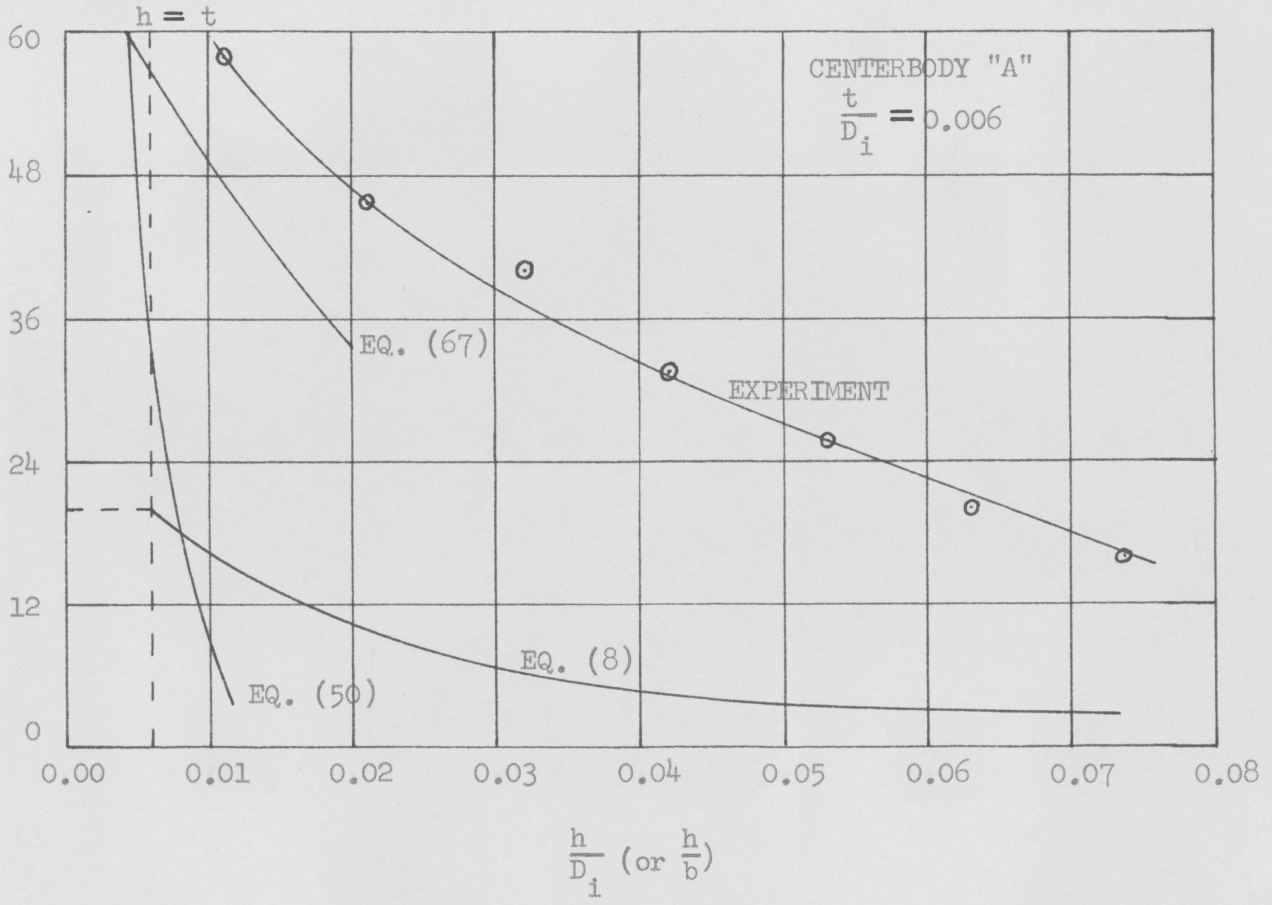


LIFT AUGMENTATION RATIO VERSUS $\frac{h}{D_i}$ (or $\frac{h}{b}$)

FIGURE 26

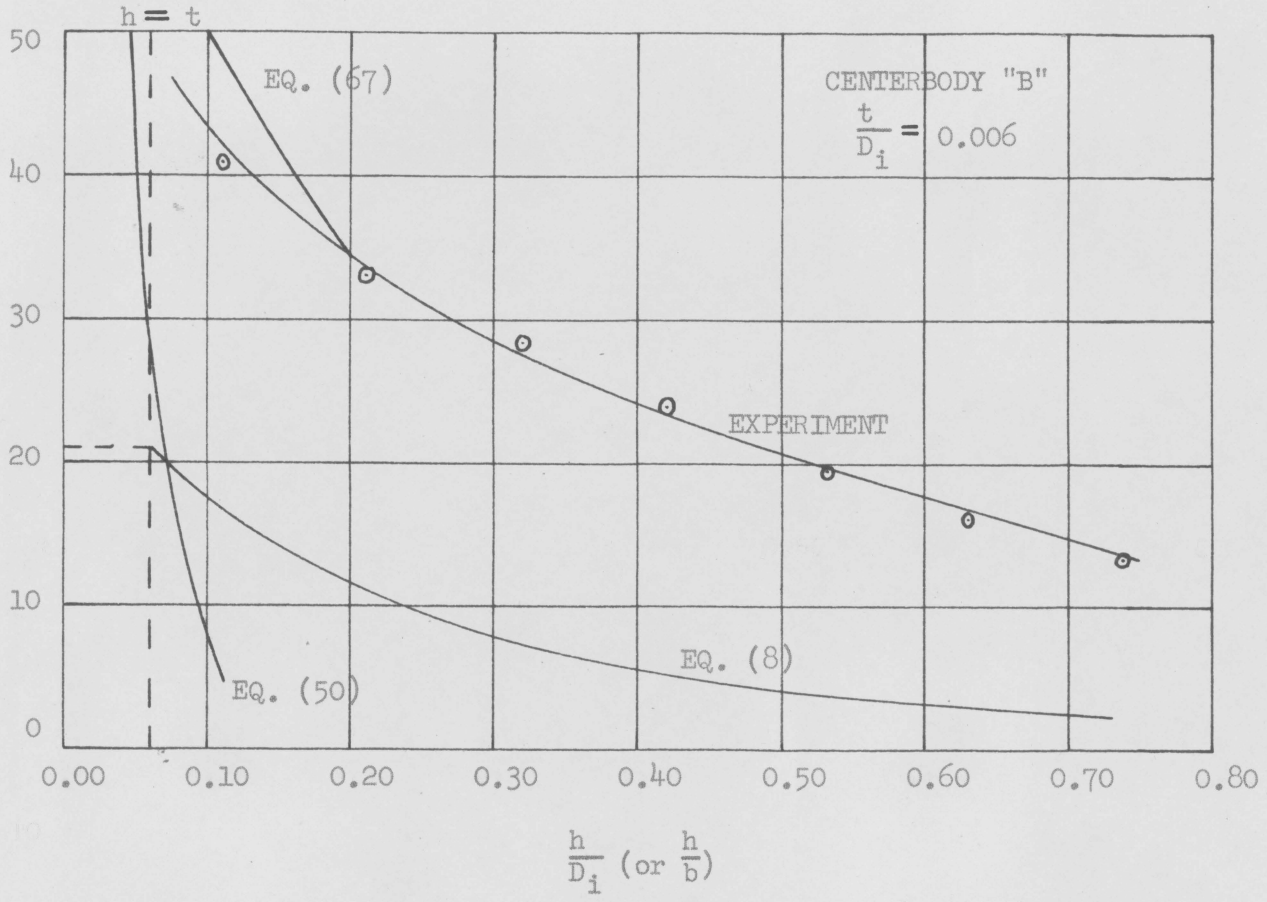


LIFT AUGMENTATION RATIO VERSUS $\frac{h}{D_i}$ (or $\frac{h}{b}$)

FIGURE 27

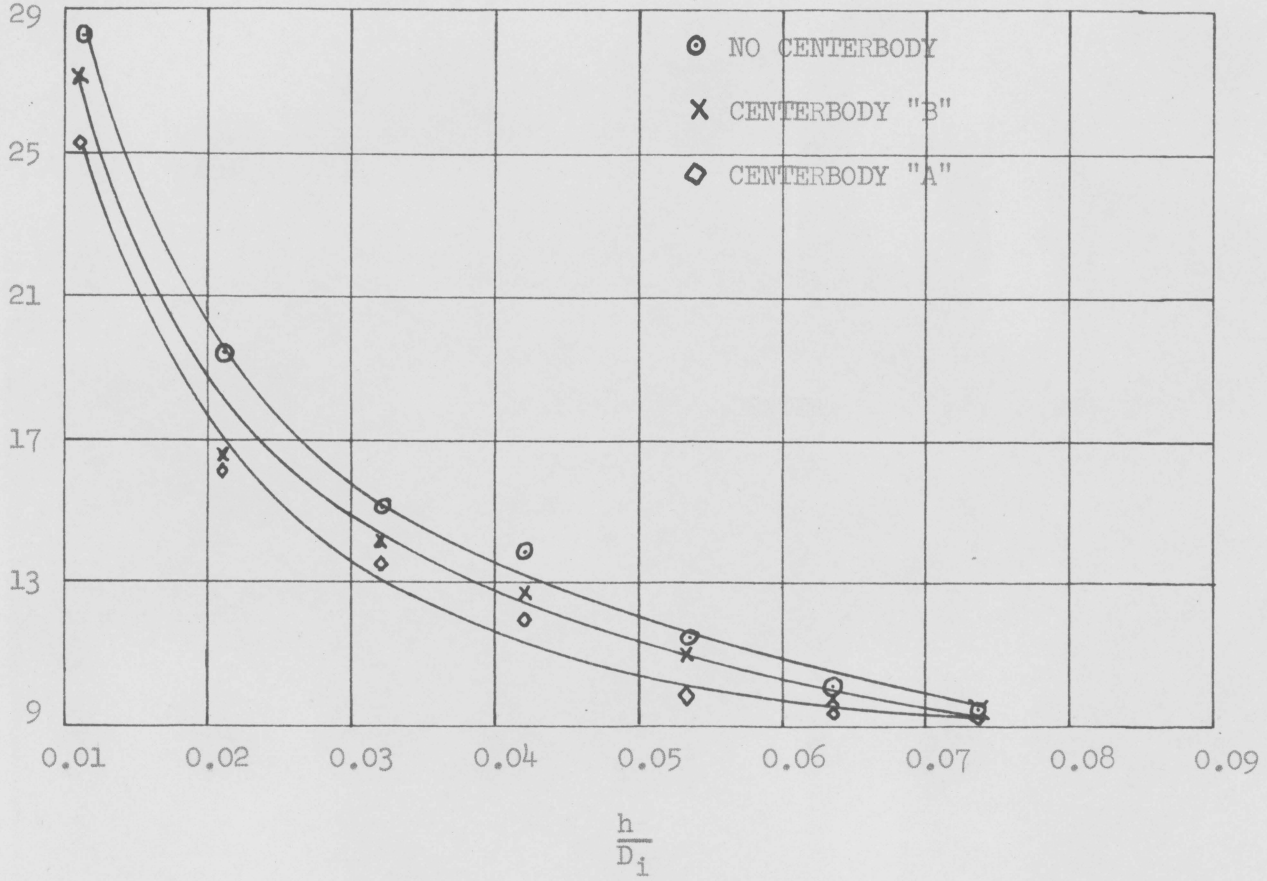


COMPARISON OF EXPERIMENTAL LIFT AUGMENTATION RATIOS FOR DIFFERENT CENTERBODY CONFIGURATIONS ($\frac{t}{D_i} = 0.032$)

FIGURE 28

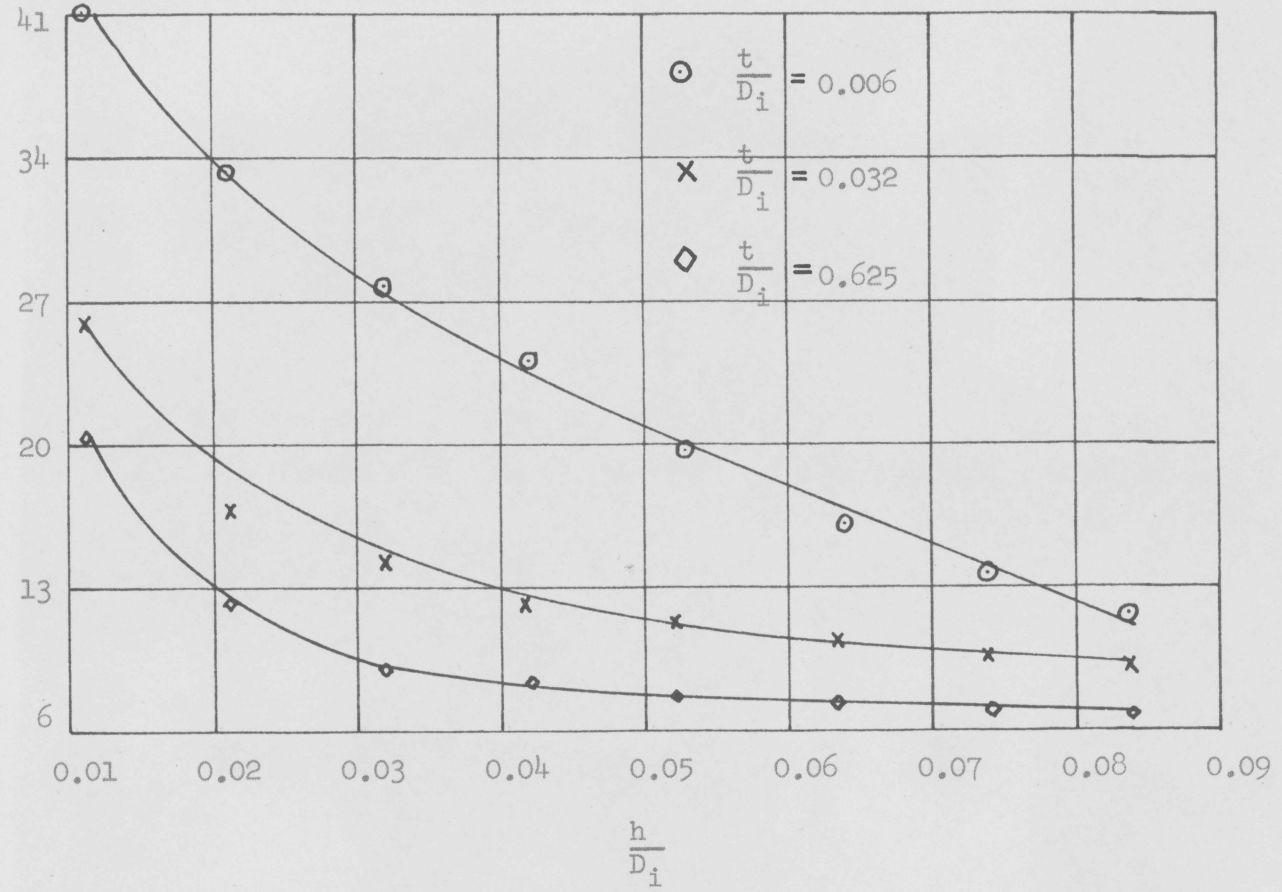


COMPARISON OF EXPERIMENTAL LIFT AUGMENTATION RATIOS FOR DIFFERENT NOZZLE THICKNESSES, USING CENTERBODY "B"

FIGURE 29

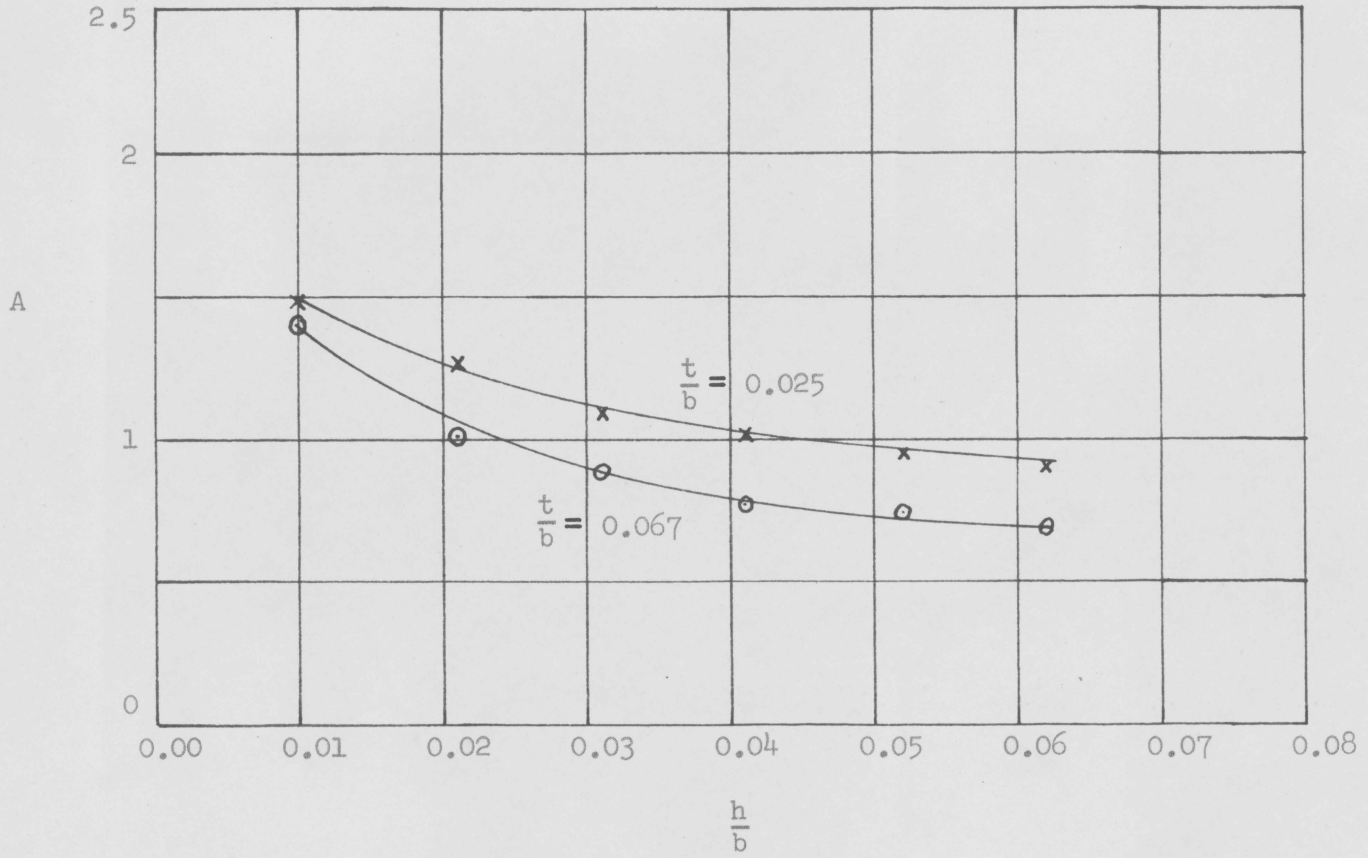


EXPERIMENTAL LIFT AUGMENTATION RATIOS OF THE "LEVAPAD" VERSUS $\frac{h}{b}$

FIGURE 30

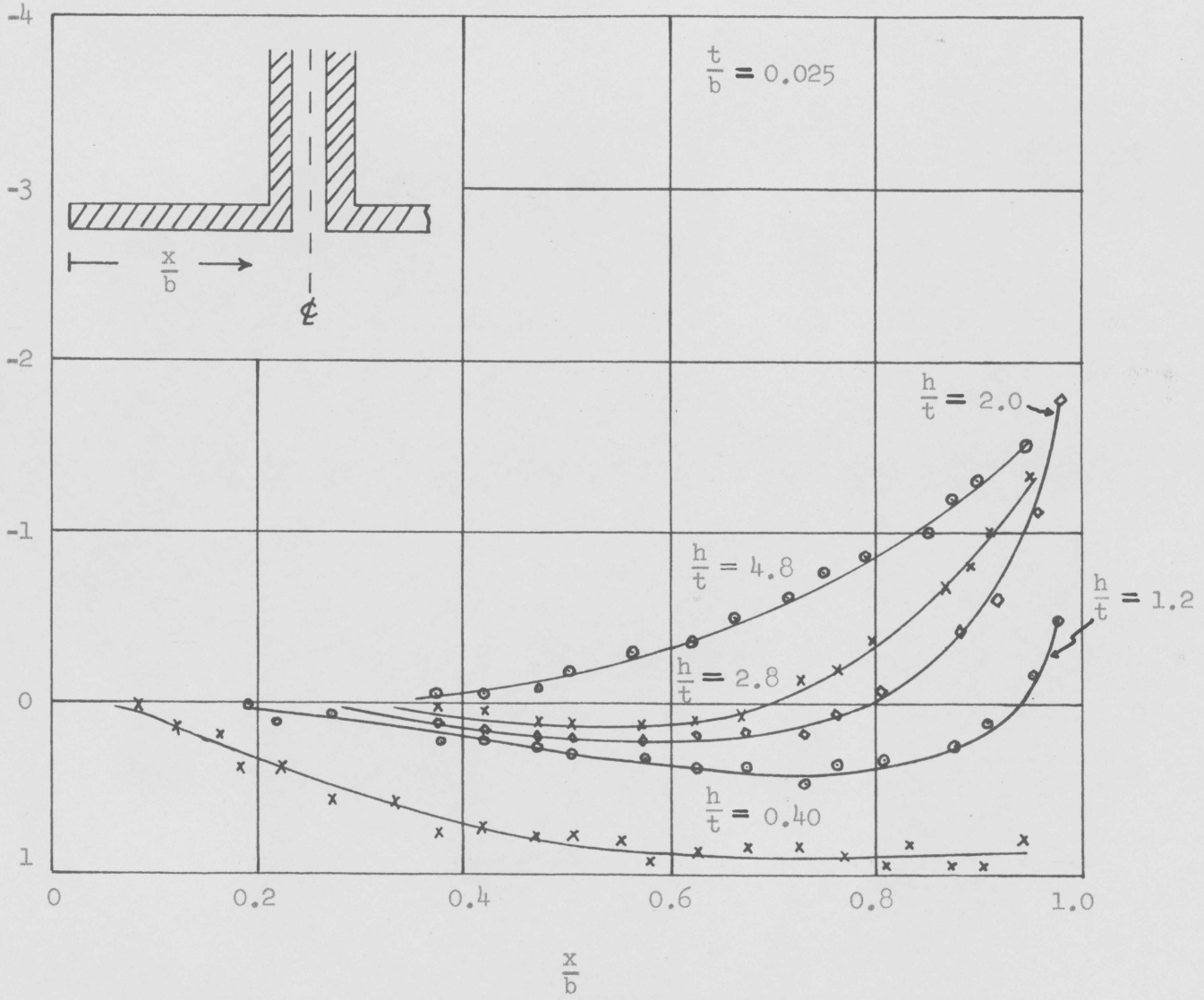


"LEVAPAD" PRESSURE DISTRIBUTION (EXPERIMENTAL) FOR VARIOUS $\frac{h}{t}$

FIGURE 31

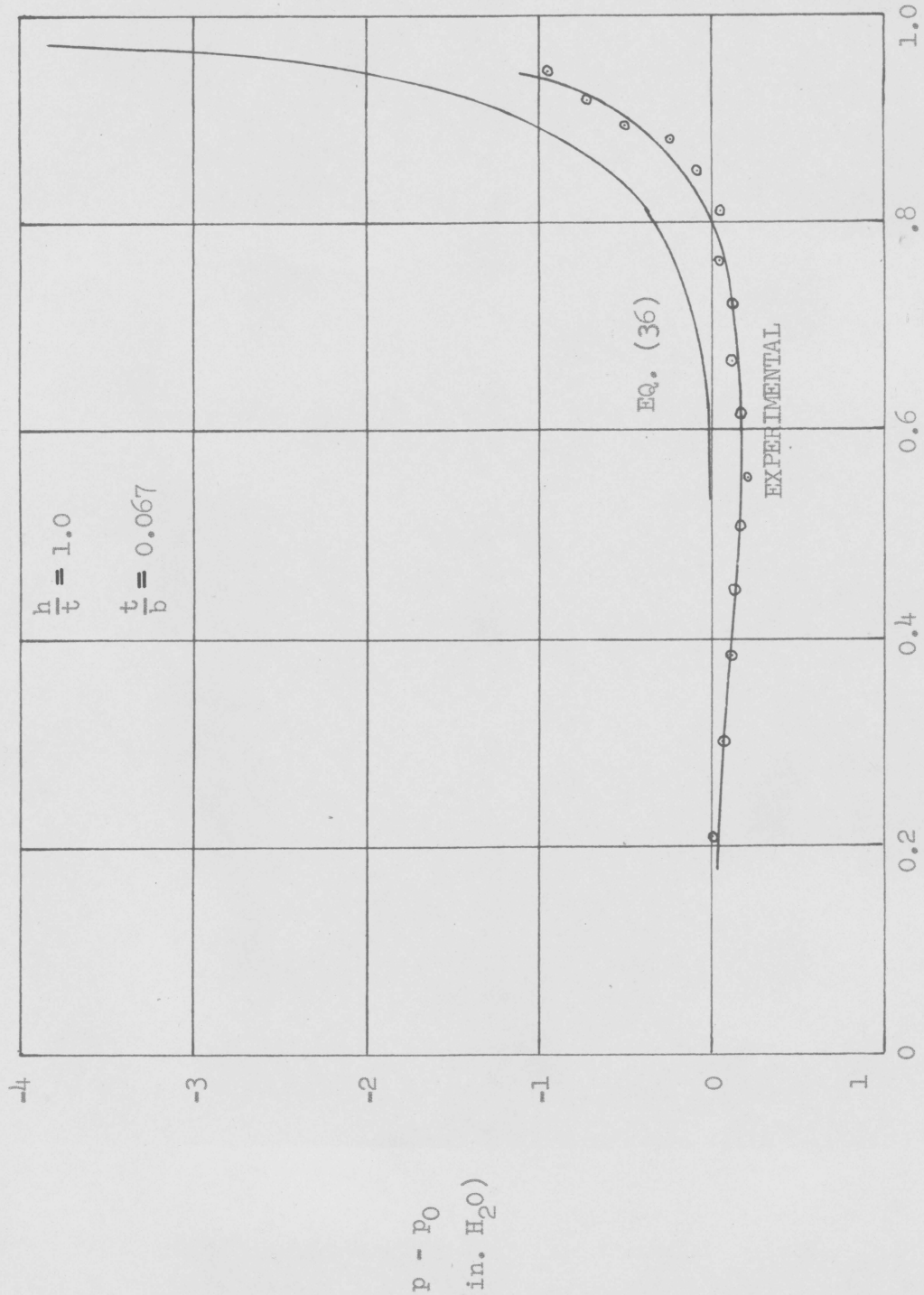


THEORETICAL AND EXPERIMENTAL "LEVAPAD" PRESSURE DISTRIBUTION

FIGURE 32

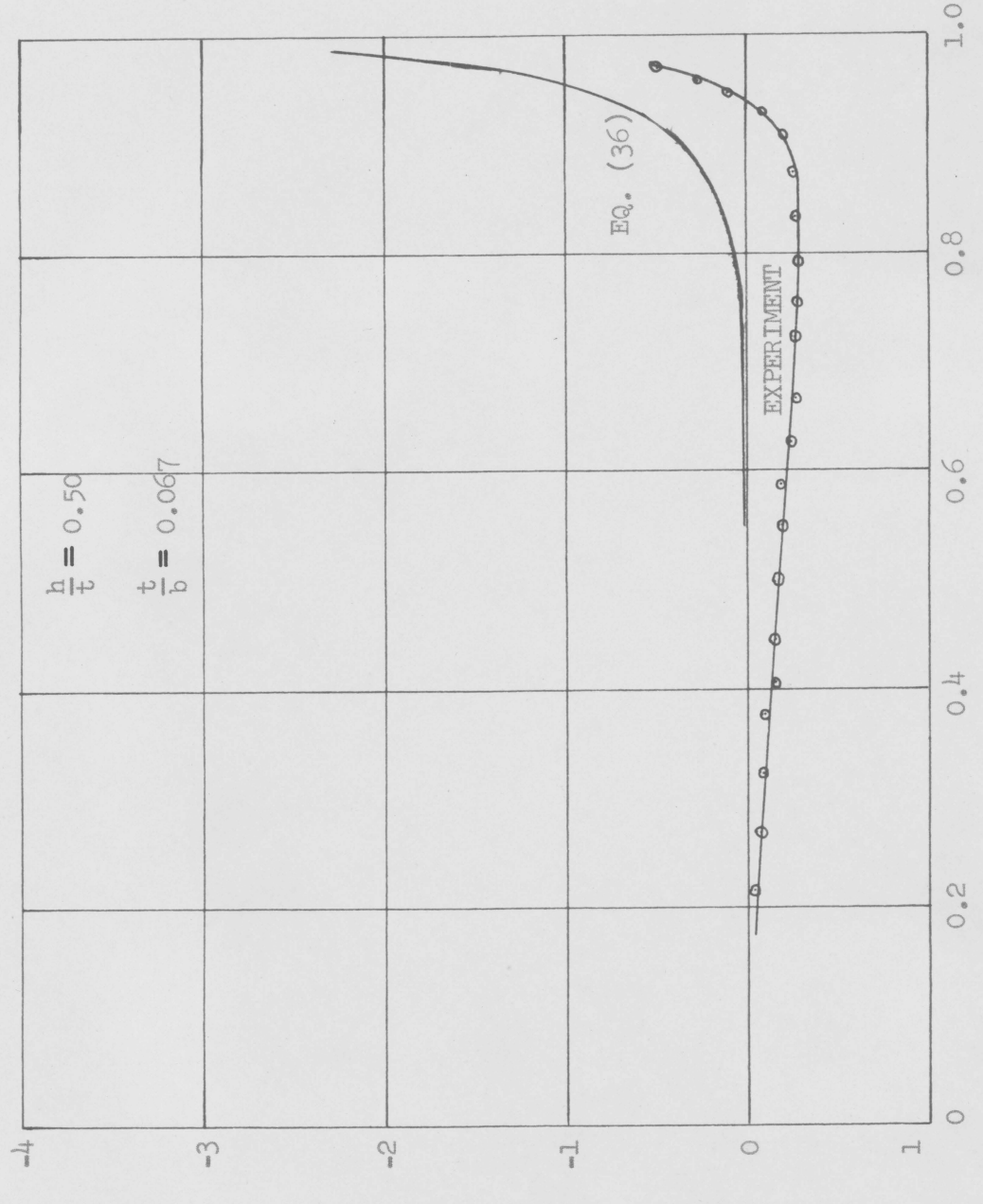


THEORETICAL AND EXPERIMENTAL "LEVAPAD" PRESSURE DISTRIBUTION

FIGURE 32a

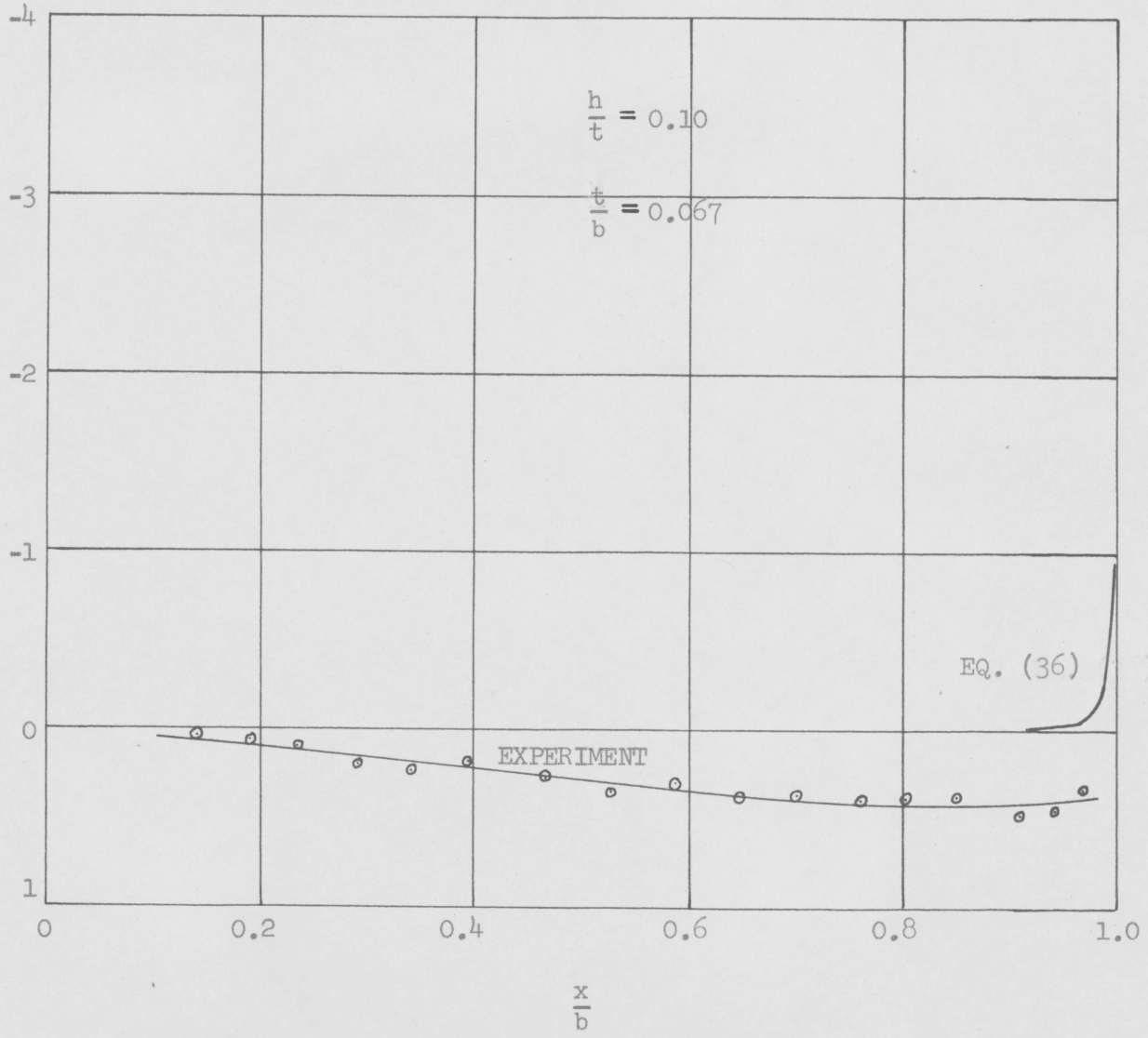


THEORETICAL AND EXPERIMENTAL "LEVAPAD" PRESSURE DISTRIBUTION

FIGURE 32b

## ABSTRACT

In this thesis expressions for the lift augmentation ratio of the two-dimensional and axi-symmetric annular jet ground effect machines are developed. These expressions account for variations of velocity and pressure across the annular jet discharge area. A Schwarz-Christoffel conformal transformation was used in the development. The only other known theory that takes into account this flow variation is invalid in the operating region of $h \leq t$. The new theory, however, is valid for all heights from approximately zero to "out of ground effect."

An axi-symmetric annular jet model was designed and constructed for experimentally obtaining lift augmentation ratios. The model was equipped with two interchangeable centerbodies of different design, and three interchangeable annular nozzle rings of different thicknesses. In all, seven different model configurations (including one "no centerbody" machine) were available. A two-dimensional "levapad" model was also constructed and tested. This model employed two interchangeable nozzles of different thickness.

All experiments were performed in the hovering condition. A constant ratio of total intake nozzle pressure to atmospheric pressure was maintained for all $\frac{h}{D}$ (or $\frac{h}{b}$) values.

Proper model design was found to be of fundamental importance in obtaining peak operating efficiency. It is believed that a

properly designed centerbody will increase the operating efficiency of these machines. A properly designed nozzle was also found to be an important factor in this respect, particularly in the two-dimensional "levapad" model.

Tuft studies were made of the jet air flow. The annular jet out of "ground effect" was observed to turn inward toward the center, an effect predicted in the literature. Also in accordance with predictions, a vortex ring was observed. In "ground effect", a portion of the annular jet was observed to flow inward, indicating that jet entrainment may be an important factor to consider in any further theoretical work.